LIQUID CRYSTAL-BASED MICROCAPILLARY SENSORS

A THESIS SUBMITTED TO
THE GRADUATE SCHOOL OF NATURAL AND APPLIED SCIENCES
OF
MIDDLE EAST TECHNICAL UNIVERSITY

BY

ELİF KURT

IN PARTIAL FULFILLMENT OF THE REQUIREMENTS
FOR
THE DEGREE OF MASTER OF SCIENCE
IN
CHEMICAL ENGINEERING

JANUARY 2022

Approval of the thesis:

LIQUID CRYSTAL-BASED MICROCAPILLARY SENSORS

submitted by **ELİF KURT** in partial fulfillment of the requirements for the degree of **Master of Science** i**n Chemical Engineering, Middle East Technical University** by,

Prof. Dr. Halil Kalıpçılar
Dean, Graduate School of **Natural and Applied Sciences** _____

Prof. Dr. Pınar Çalık
Head of the Department, **Chemical Engineering** _____

Asst. Prof. Dr. Emre Büküşoğlu
Supervisor, **Chemical Engineering, METU** _____

Examining Committee Members:

Prof. Dr. Nihal Aydoğan
Chemical Engineering, Hacettepe University _____

Asst. Prof. Dr. Emre Büküşoğlu
Chemical Engineering, METU _____

Assoc. Prof. Dr. Erhan Bat
Chemical Engineering, METU _____

Asst. Prof. Dr. Simge Çınar Aygün
Metallurgical and Materials Engineering, METU _____

Asst. Prof. Dr. Gökçe Dicle Kalaycıoğlu
Chemical Engineering, Hacettepe University _____

Date: 21.01.2022

I hereby declare that all information in this document has been obtained and presented in accordance with academic rules and ethical conduct. I also declare that, as required by these rules and conduct, I have fully cited and referenced all material and results that are not original to this work.

Name, Last name : Elif Kurt

Signature :

ABSTRACT

LIQUID CRYSTAL-BASED MICROCAPILLARY SENSORS

Kurt, Elif
Master of Science, Chemical Engineering
Supervisor: Asst. Prof. Dr. Emre Büküşoğlu

January 2022, 73 pages

Stimuli-responsive properties of liquid crystals (LCs), when combined with their optical properties, offer sensitive and rapid sensing applications. In the first part of this thesis study, we propose and demonstrate a microcapillary-based method to be applied for the online detection of amphiphilic species, which can be further used for biological and chemical species in aqueous media. Specifically, we used compartments (300-1400 μm) of nematic 4-cyano-4'-pentylbiphenyl (5CB) that is positioned into cylindrical shaped glass microcapillaries that promote homeotropic anchoring. The flat surfaces of the cylindrical LC compartments were in contact with an aqueous media. We characterized the equilibrium and nonequilibrium response of LC upon a change in the anchoring of LCs at the LC-aqueous interfaces. Upon anchoring transition, we observed a formation of a positively charged defect at the proximity of the interface that moved to the center of the LC compartment and reached equilibrium, four-petal configuration. This transition was observed to take an average of 41±19 min., which was significantly larger than the time that would take for diffusion and adsorption of the surface-active species at LC-water interfaces. We concluded this to relate to the motion of the defect due to the imbalance of the elastic forces. During the transition, we observed metastable states which could be

removed via thermal treatment. We showed that the capillary sensors to be more advantageous over the flat film counterparts in terms of the ease of quantification. We also show that the sensors are reversible that facilitates temporal and cumulative quantification. In the second part of this thesis study, we developed aptasensors to be used in both flat and microcapillary geometries. We sequentially functionalized the glass surfaces first with mixed monolayer of (3-Aminopropyl)triethoxysilane (APTES) and dimethyl octadecyl [3-(trimethoxysilyl) propyl] ammonium chloride (DMOAP), then glutaraldehyde solution (GA) to immobilize neomycin aptamer via glutaraldehyde linkage method. Through the binding of aptamer to its target molecule, the conformation of aptamer was changed resulting in the LC configuration transition from homeotropic to degenerate planar/tilted which we visualized under polarized optical microscope. The detection limit for both geometries was found to be in between 50-500 nM neomycin B concentrations. We exposed sensors to different target solutions consisting of neomycin B and ampicillin, and carried out qualitative and quantitative analyzes. The findings reported in this thesis can further be used to develop sensors for specific purposes that require continuous tracking of the chemical and biological species that is critical for the health and safety of the individuals and society.

Keywords: Liquid Crystals, Microcapillary, Aptamer, Optical Sensor, Biosensor

ÖZ

SIVI KRİSTAL BAZLI MİKROKAPİLER SENSÖRLER

Kurt, Elif
Yüksek Lisans, Kimya Mühendisliği
Tez Yöneticisi: Dr. Öğretim Üyesi Emre Büküşoğlu

Ocak 2022, 73 sayfa

Sıvı kristallerin uyaranlara duyarlı özellikleri, optik özellikleriyle birleştirildiğinde hassas ve hızlı algılama uygulamaları sunar. Tez çalışmamızın ilk aşamasında, sulu ortamdaki biyolojik ve kimyasal türler için ayrıca kullanılabilecek amfifilik türlerin çevrimiçi tespiti için uygulanacak mikro kılcal tabanlı bir yöntem öneriyoruz ve gösteriyoruz. Spesifik olarak, homeotropik çapalamayı destekleyen silindirik şekilli cam mikro kapilerlere yerleştirilmiş nematik 4-siyano-4'-pentilbifenil (5CB) bölmeleri (300-1400 μm) kullandık. Silindirik sıvı kristal bölmelerinin düz yüzeyleri, sulu bir ortam ile temas halindeydi. Sıvı kristal-sulu arayüzlerde sıvı kristallerin sabitlenmesindeki bir değişiklik üzerine sıvı kristalin denge ve dengesizlik tepkisini karakterize ettik. Çapalama geçişi üzerine, sıvı kristal bölmesinin merkezine hareket eden ve dengeye, dört yapraklı konfigürasyona ulaşan arayüzün yakınında pozitif yüklü bir kusur oluşumunu gözlemledik. Bu geçişin ortalama 41±19 dakika sürdüğü gözlemlendi; bu, yüzey aktif türlerin sıvı kristal-su arayüzlerinde difüzyonu ve adsorpsiyonu için gereken süreden önemli ölçüde daha uzundu. Bunun, elastik kuvvetlerin dengesizliğinden kaynaklanan kusurun hareketiyle ilgili olduğu sonucuna vardık. Geçiş sırasında, ısıl işlemle giderilebilecek yarı kararlı durumlar gözlemledik. Kapiler sensörlerin kantifikasyon kolaylığı açısından düz film muadillerine göre daha avantajlı olduğunu gösterdik. Ayrıca,

sensörlerin zamansal ve kümülatif nicelemeyi kolaylaştıran tersine çevrilebilir olduğunu da gösterdik. Bu tez çalışmasının ikinci bölümünde hem düz hem de mikrokapiler geometrilerde kullanılmak üzere aptasensörler geliştirdik. Cam yüzeyleri ilk önce (3-Aminopropil)trietoksisilan (APTES) ve dimetil oktadesil [3-(trimetoksisilil) propil] amonyum klorür (DMOAP) karışık tek katmanı , ardından neomisin aptameri glutaraldehit bağ yöntemi ile immobilize etmek için glutaraldehit (GA) solüsyonu ile fonksiyonladık. Aptamerin hedef molekülüne bağlanması yoluyla, aptamerin konformasyonu değiştirilir, bu da sıvı kristal konfigürasyonunun polarize optik mikroskop altında görselleştirdiğimiz homeotropikten dejenere düzlemsel/eğikliğe geçişiyle sonuçlanır. Her iki geometri için de algılama sınırının 50-500 nM neomisin konsantrasyonları arasında olduğu bulunmuştur. Sensörleri neomisin ve ampisilin içeren farklı hedef karışımlara maruz bıraktık ve nitel ve nicel analizler gerçekleştirdik. Bu tezde bildirilen bulgular ayrıca, bireylerin ve toplumun sağlığı ve güvenliği için kritik olan kimyasal ve biyolojik türlerin sürekli izlenmesini gerektiren belirli amaçlar için sensörler geliştirmek için kullanılabilir.

Anahtar Kelimeler: Sıvı Kristaller, Mikrokapiler, Aptamer, Optik Sensör, Biyosensör

To my beloved family…

ACKNOWLEDGMENTS

To begin with, I would like to express my deepest gratitude to my supervisor, Asst. Prof. Dr. Emre Büküşoğlu, for his guidance, encouragements, support and enlightenment throughout this thesis study. I truly appreciate the time, effort and patience he has given in every aspect of this valuable experience. I must also express my gratitude to Dr. Müslüm İlgü for his helpful suggestions, support and guidance.

I would also like to say a special thank you to all the Soft and Functional Materials Laboratory Group members; Aslı Karausta, Özge Batır, Burak Akdeniz, Deniz Avşar, Ceren Kocaman, Selin Şengül, Umut Dinç, Elif Erçelik, Ali Akman and Pınar Beyazkılıç Ayas for their endless support and friendship and also being my emergency accommodation, transportation and healthcare services in Ankara. I am grateful to you for being not just lab mates but true friends. You are my source of happiness making me come with joy every morning.

I am fortunate to have my dearest friends who always supported me. I want to thank to Toprak Çağlar and Çağla Bozcuoğlu for their friendship and support throughout these three years. Also, I would like to thank my homie, Ceren Başer Kanbak, for making our home a warm place to live and all her support in everything we went through. Especially, I would like to thank to İrem Öztürk, who was always there for me in all those METU years with her endless support and love. I feel very lucky to have you in my life, we have a very long road ahead of us. From the bottom of my heart, I would like to say a big thank you to Tuğçe Savran and Nisan Yüce for their caring, love, support and encouragement for all these years. The distance means nothing when the hearts are together, thank you sisters for showing this in every single day. I do not know what I would do without you, yet I know that this will last forever. My biggest thanks go to my childhood; Berkhan Ağar, Selin Çalıcıoğlu and Onur Şen. It has been twenty years, and I know that we will always be there for us

no matter what happens, no matter how far we are. You are my past and my future, you are my chosen family.

Last but not the least, I would like to express my sincere and deepest appreciation to my lovely family for their endless, unconditional love and being my biggest supporters. My beloved ones, I simply couldn’t have done this without you. İsmihan Güney Kurt, thank you for making me feel like I have a sister from the beginning of my life though we spent most of our lives apart. Erdem Cemil Kurt, you are the greatest brother a girl can ask for. I've known since I was a baby that as long as you're by my side, I'll always be safe. Hatice Kurt and Şeref Kurt, I am very lucky to have mom and dad like you. In this year of my 8-year Ankara journey, I realized once again that I am stronger when you are with me. I will always be proud of being your daughter!

This work was supported by the Scientific Research Projects Coordination of the Middle East Technical University under the grant number GAP-304-2021-10608.

TABLE OF CONTENTS

LIST OF FIGURES

FIGURES

CHAPTER 1

INTRODUCTION

Sensing and the quantification of chemical and biological species have been studied for many years. For these purposes, there are standard, reliable and conventional analytical methods like high-performance liquid chromatography (HPLC), gas chromatography-mass spectrometry (GC-MS), Enzyme-Linked Immunosorbent Assay (ELISA) and etc.; however, most of these methods require long times for detection, bulky and expensive instrumentation and do not allow label-free detection of samples. [1–3]

To make a sensing method preferrable among other techniques, there are requirements that need to be fulfilled. The most wanted feature of a sensor is rapid responses to decrease the waiting time. Easy sampling is also needed to make the preparation part easier and less time consuming. Easy fabrication is desirable for minimizing errors from materials and production. High stability and sensitivity are desired for consistency, durability and obtaining sensitive sensors. Finally, label-free detection and reusability are required to decrease the operation and material costs as much as possible for continuous measurements.

Liquid crystal (LC)-based sensors are one of the strong candidates owing to their sensitive response and optical properties. They offer simpler, inexpensive, and passive sensing platforms that take advantage of optical reporting of the events occurring at their interfaces.[4] Also, optical responses obtained from the interfacial interactions between the LC mesogens and the targeted species makes them promising platforms for specific biosensing applications.[1,5–9]

LCs are phases of matters between crystalline solids and isotropic liquids, which show both long-range orientation ordering and mobility. If the phase behavior changes with respect to temperature, LCs are named as thermotropic where the mobility of LC mesogens increase with increasing temperature (See Figure 1.1). In nematics, which is the simplest phase of LCs, molecules have an average orientational order in the same direction which is called as nematic director; but they do not show long-range positional order.[10,11]

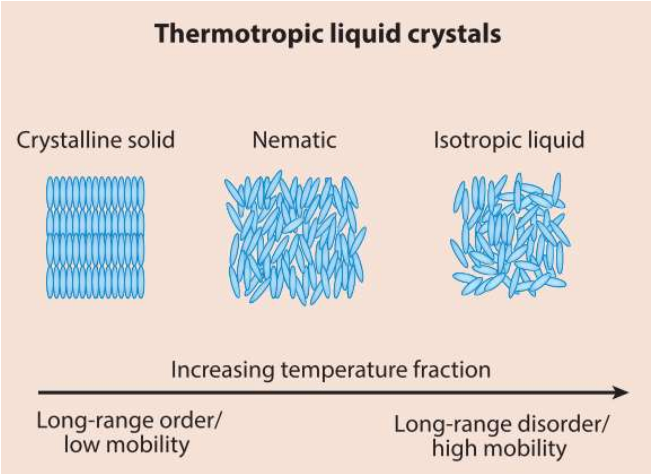

Figure 1.1 Schematic illustration of the phase behavior of thermotropic liquid crystals from crystalline solid to isotropic liquid with the increasing temperature. [11]

There are three key concepts apply to LCs which are surface anchoring, elasticity and the formation of topological defects (Figure 1.2).[11] Intermolecular interactions between the LCs and the confining medium give an order to LCs which can be explained with the surface anchoring phenomenon. Easy axis is the lowest free energy orientation of LC director which is observed when no external field is applied. Deviation of the director from easy axis resulting from an applied external field leads to an increase in the free energy of the interface, which can be described as;

$$F_s = F_0 + \frac{1}{2} W_a sin^2(\theta_s - \theta_e) \qquad \text{(Equation 1)}$$

where W_a represent the surface anchoring energy, θ_s is the angle defining the surface director orientation while θ_e is the angle defining the easy axis orientation, and F_s

and F_0 are the free energy of the interface and free energy of the interface which corresponds to the easy axis, respectively.

Elastic properties of LCs provide the long-range orientational ordering property to LCs. Splay, twist and bend are the three main modes of strain observed in LCs which give the LCs elasticity. Free energy density of the LCs can be described by the Frank-Oseen equation below, where K_1, K_2 and K_3 are the elastic constants for splay, twist and bend strain modes;

$$F_d = \frac{1}{2}K_1(\nabla \cdot n)^2 + \frac{1}{2}K_2(n \cdot \nabla \times n)^2 + \frac{1}{2}K_3(n \times (\nabla \times n))^2 \quad \text{(Equation 2)}$$

The final key concept relevant to LCs is the formation of topological defects. When confined in defined geometries, LC locally melts because of the highly strained regions within LC phase. Thus, topological defects are formed to maintain surface-induced ordering and alignment. With these characteristics, LCs take advantage of optical reporting of the events occurring at their interfaces. By means of this, they can be integrated in stimuli-responsive sensing applications where they are used as optical amplifiers.

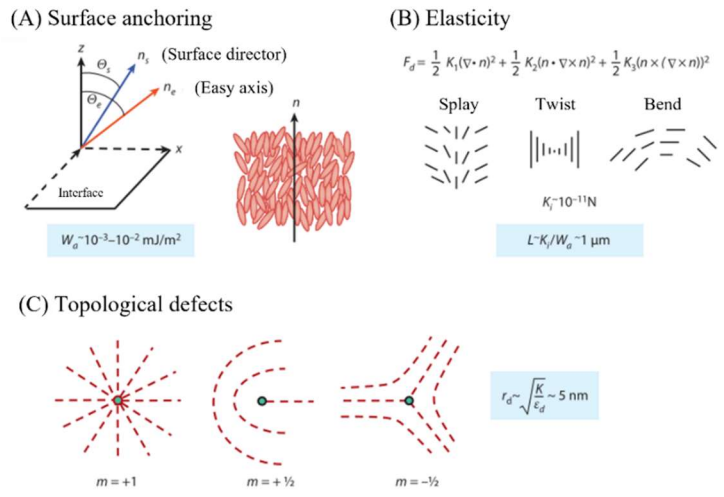

Figure 1.2 Schematic illustration of three key concepts of LCs. (A) Anchoring of the director and the easy axis of LC at the surface, (B) the three main modes of strain of LC and (C) three types of topological defects that can form in LC: (left) a point defect located at the center of a radially converging director field, and (center, right) cross-sections of line defects (disclinations). [11]

Having long-range orientational ordering makes LCs optically anisotropic materials. They show optical birefringence property, possessing two different refractive indices, which allows to determine the orientation of LCs under crossed polarizers by affecting the polarization of transmitted light. [10,11] Interaction of LC mesogens with chemical or biological species can induce an ordering transition of the LC phase due to the long-range ordering property of the LCs and it can be viewed through polarized optical microscope (POM). Having mobility, which is generally interrelated with isotropic liquids, provides reorganization and communication within the LC phase.

Past studies investigated the use of solid and aqueous interfaces for the sensing and characterization of analytes in various environments where LCs were used in different forms. To date, LC-based sensors have been successfully applied to detect a range of species including glucose[12–14], metal ions[15,16], surfactants[17–20], proteins[21,22], enzymes[23], phospholopids[24,25], cholesterol[3], viruses[26,27], and living cells[28]. The detection limit of some of these LC-based sensors can reach up to picogram per milliliter levels.[9,29] So far, the initial and final configurations and characterizations were studied. Most recently, acquiring time-dependent information of transition states gained importance.[30–32]

Lately, for the specific recognition purposes, aptamer-based biosensors have been developed. Aptamers are single stranded DNA or RNA molecules that selectively bind to its target with high sensitivity and affinity. They can be used several times after regeneration without major loss of activity. Also, they are stable molecules and can be synthesized inexpensively with high purity and reproducibility.[33–36]

Here in the first part of this thesis study, we seek to develop a portable sensing system to be used for the online detection and characterization of chemical and biological species, observe the defect motion within LC phase and obtain fundamental information of transition states. For this purpose, we used microcapillary-based system where we benefit from the interfacial interactions between the order of hundred microns-sized, pre-formed LC compartments and aqueous media. We show

that the LC compartments respond to the changes occurring at their interfaces resulted from the interactions with analytes. We performed optical characterizations and measured the response with respect to various model analyte concentrations and time. The proposed system offers reversibility and two separate, independent LC-aqueous interfaces that could be used for analytical purposes and online measurements. Also, understanding of transition states with time-dependent defect motion can further be used for image processing-machine learning purposes. For the second part of the thesis study, we wanted to develop a LC-based aptasensor to be used both in flat and microcapillary geometries. After successive surface functionalization and aptamer immobilization, we created reactive sites on the glass surfaces for target molecules to bind specifically its aptamer. The limit of detection of proposed aptasensor reached up to nanogram per milliliter levels for both geometries. We exposed sensors to different target solutions consisting and carried out qualitative and quantitative analyzes. Overall, the LC microcapillary-based sensors offer easy quantification, label-free and affordable platforms to be widely used in tracking of chemical and biological species.

CHAPTER 2

LITERATURE REVIEW

Stimuli-responsive properties of LCs makes them promising materials for sensing applications. To date, there have been successful studies proposed regarding LC-based sensors for detection of various species like surfactants, lipids, bacteria and viruses without the need for a labeling agent or heavy and complex instrumentation. Within these studies, chemically functionalized solid surfaces or LC-aqueous interfaces allowing adsorption of analytes from different environments used for the detection and quantification purposes. [4,24,37]

Formerly, LC-based sensing platforms have been developed for the detection of various species utilizing LC-solid interfaces.[1,5,6,26,38–42] In these methods, functionalization of the surfaces with analytes like proteins[39], polymers[40], peptides[41] among others and the incubation are the crucial steps. In a study, Bai et al. investigated the LC behavior on dipeptide-decorated gold surfaces supported with glass slides. [43]. With the formation of monolayers of L-cysteine-L-tyrosine, L-cysteine-L-phenylalanine, or L-cysteine- L-phosphotyrosine, they observed that patterns of hydrogen bonding specific to the tyrosine monolayers orient the LCs as well as the phosphorylation of tyrosine. Also, they reported that stereoisomerism plays a role since it influences the chemical group patterning of dipeptides forming monolayers. As an another example for sensors utilizing LC-solid interfaces, Chen et al. reported a LC-based method to detect surface-immobilized DNA with a limit of detection approximately 4 μg/mL by using 10 nL of DNA solution. [42] In a recent study, Ren et al. proposed a LC-based biosensor for the detection of bisphenol A (BPA) by using sequentially functionalized glass surfaces. [1] They modified the glass surfaces with mixture of silane groups (dimethyl octadecyl [3-(trimethoxysilyl)

propyl] ammonium chloride (DMOAP) and (3-aminopropyl)triethoxysilane (APTES)) and immobilized the BPA aptamer on the glass surfaces via glutaraldehyde linkage. Until the immobilization of aptamer, they observed dark appearance under polarized optical microscope (POM) which indicates the homeotropic orientation of LCs at the glass surfaces. With the specific binding of BPA aptamer to its target, they observed a bright appearance under POM which is the indicative of orientation transition from homeotropic to planar as shown in Figure 2.1.

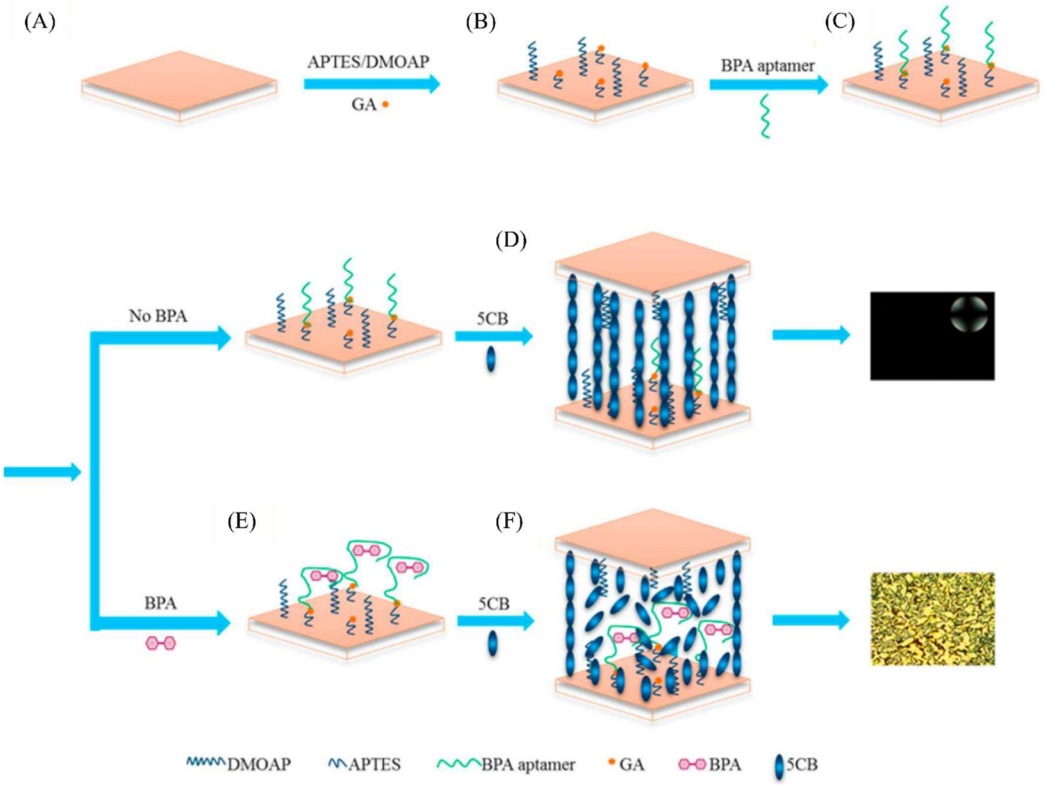

Figure 2.1 Schematic illustration of LC-based biosensor for the detection of BPA. (A) piranha-treated glass slide, (B) surface functionalization with APTES/DMOAP mixture, (C) immobilization of BPA aptamer via glutaraldehyde linkage, (D) homeotropic alignment of LC at the inner surfaces of optical cells in the absence of BPA, (E) incubation of glass slides with BPA solution and (F) random orientation of LC in optical cells after surface treatment with BPA. [1]

This method is widely used; however, it is challenging to implement to the online measurements or applications that require fast response. Also, although they form

useful systems, LC-solid interfaces have some disadvantages compared to LC-aqueous interface counterparts. First, LC-aqueous interfaces offer higher mobility of the molecules which allow the molecules to reorganize laterally upon adsorption to the interface. Influenced by the elastic properties of LC molecules, interfacial phase states of the molecules can be observed with the organization of the molecules at the LC-aqueous interfaces. Second, LC-aqueous interfaces are soft and deformable contrary to LC-solid interfaces.[4] Based upon these advantageous characteristics, LC-aqueous interfaces are promising for the LC-based sensing applications. One of the form of LC-based sensors where LC-aqueous interface can be obtained is LC on solid surface in contact with a fluid media.[3,12–14,16,23,44–46] One of the most advantageous feature of this method is providing time-dependent ordering transition analysis.[23,30,31] Park et al. reported a method to conjugate the oligopeptides LC-aqueous interface.[23] They used a gold electron microscopy grid to confine LC on the octyltrichlorosilane (OTS)-functionalized glass slides to give homeotropic orientation to LCs at solid surface and immersed it in aqueous media to obtain LC-aqueous interface. 17-amino-acid oligopeptides are conjugated to a mixed monolayer of tetra(ethylene glycol)- containing lipid ($CH_2(CH_2)_{13}(OCH_2CH_2)_4OH$) and a carboxylic acid-terminated lipid ($CH_2(CH_2)_{13}(OCH_2CH_2)_4OCH_2CO_2H$) through N-hydroxysuccinimide (NHS)-activation of carboxylic acid groups. After the formation of lipid domains at the interface, dark images were obtained under POM which indicates the homeotropic anchoring of LC mesogens at the LC-aqueous interface, while they assume planar anchoring when there is no lipid present in aqueous media. With the immobilization of 17-amino-acid oligopeptides, orientation transition from planar to homeotropic was observed. They later used trypsin to cleave the oligopeptides which resulted in again homeotropic alignment of LCs at the interface (Figure 2.2). With the conjugation of oligopeptides to the interface and the cleavage, they investigated optically the real-time responses of interfacial enzymatic interactions.

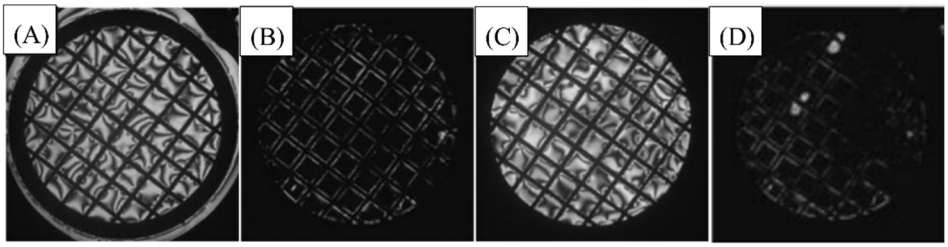

Figure 2.2 Optical images of nematic 5CB (A) in contact with PBS buffer (pH=7.6), (B) after incubation with aqueous lipid mixture in PBS buffer (pH=7.6), (C) after immobilization with aqueous solution of the 17-amino-acid oligopeptide in PBS (pH=7.6), (D) after contact of the oligopeptide-decorated interface with trypsin. [23]

Despite the fact that the method of LC on solid surface contacting with fluid media allows time-dependent analysis, they are not suitable for flexible and long-term use due to the changes observed on the reference surface under some circumstances as Yang et al. reported in their study. [47] They reported the observations of water droplets formation depending on the surface charge density and the electrolyte concentration. When they used OTS-treated glass slides to support the gold grid filled with nematic LC and immersed it in water, they observed spontaneous nucleation and growth of water droplets at the solid-LC interface which directly affects the optical response as can be seen in Figure 2.3. However, there are no water droplets formed on mixed alkanethiol monolayers ($C_{10}SH$ and $C_{16}SH$) on gold film which possess positive ζ-potential values in water whereas OTS-treated surfaces possess negative ζ-potential. They also reported that the formation of water droplets can be minimized with high solute concentrations, yet, this will have a great effect on sensor response. Because of these reasons, they may not be useful for every system. In addition, these solid-LC interface-based methods do not provide free interfaces at both sides of LC for analyte exchange between the LC interface and the bulk which limits their application for analytical purposes.

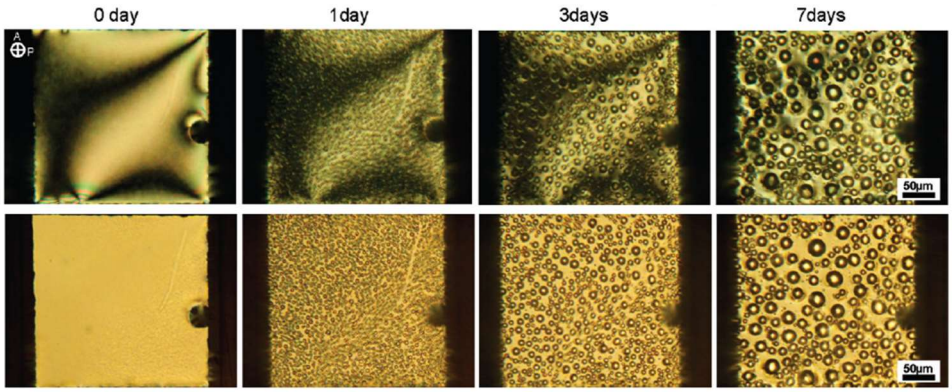

Figure 2.3 Optical images of LC in gold grids supported on OTS-treated glass slides in contact with water for 7 days at high magnification. The top row belongs to the polarized light images (crossed polars), and the bottom row belongs to bright field images. [47]

LC-in-water emulsions are another most preferred applications of LC-aqueous interfaces. In a study, Gupta et al. examined monodisperse LC droplets to characterize the ordering transitions induced by the adsorption of amphiphiles at the LC-aqueous interface. [48] They used silica templated poly(styrene sulfonate) (PSS) and poly(allyamine hydrochloride) (PAH) polymeric multilayer shells to produce predetermined sizes of monodisperse LC droplets and sodium dodecylsulfate (SDS) as the amphiphile (Figure 2.4). The PSS/PAH-encapsulated LC droplets showed bipolar configuration in the absence of SDS molecules. As the SDS concentration increases, they observed continuous orientation transition from planar to homeotropic which results in final radial configuration. They identified six equilibrium configuration states of LC droplets as a function of increasing SDS concentration.

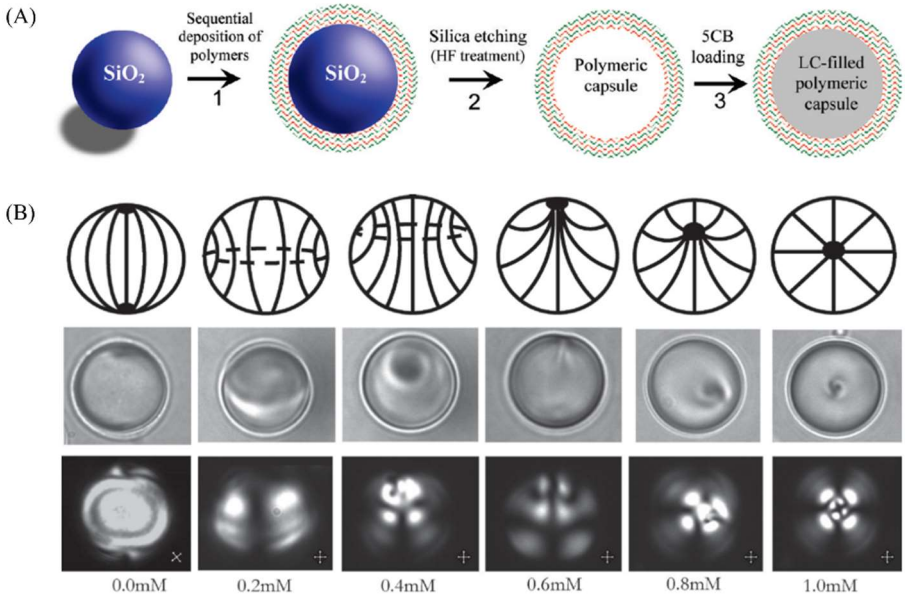

Figure 2.4 (A) Schematic illustration of preparation procedure of polymer-encapsulated LC droplets, (B) Schematic illustration and optical images of equilibrium states of LC droplet with increasing concentration of SDS solution from 0.0 mM to 1.0 mM. [48]

Sensing methods based on LC droplets offer good sensor applications. They are highly mobile, and due to the spherical geometry, sensitivity of droplet-based LC sensors is high. However, droplets are in motion leading to be not easy to follow. Also, characterizations in these methods are not easy as the number of the droplets counted should be high for robust and reliable results. Lately, Miller et al. investigated the use of flow cytometry for automated characterization of the LC droplets.[49] Compared to use of optical microscopy, results are satisfactory for obtaining faster and robust analyses. However, the translational and rotational thermal motion of the droplets usually prevents fast quantification in an economical way, it requires an additional instrumentation which is not desired for developing simple and affordable sensor applications.

More recently, LC-based microcapillary sensors are being studied.[9,50,51] Since the aspect ratio of the microcapillary is high, they can be taken as enclosed materials. Owing to this, environmental changes can be minimized leading to rather easier technique for sensing applications. Also, microcapillary-based methods provide both

solid-LC and aqueous-LC interfaces to be used for the sensing of different analytes from various environments. In a recent study, Zhong et al. reported an experimental system for confining LC in microcapillaries for the development of an optical sensor.[51] They used glass microcapillaries whose inner surfaces were functionalized with OTS to give homeotropic anchoring to LC mesogens. In this system, 5CB is used as LC phase and siphoned into the capillary by the use of capillary effect. Under these circumstances, an escaped radial configuration within LC compartment was observed. With a needle connected to a pipe, the solution of interest syringed inside the capillary and divided the LC phase into compartments without control over their sizes and locations. When they used a surfactant solution as the aqueous phase, they observed a characteristic four-petal appearance which indicates homeotropic anchoring of LC mesogens at both sides of the LC compartment. In contrast to, when the solution was free of surfactant, they observed no change on the configuration within LC phase which indicates the planar anchoring at both sides of LC phase. They inserted a full wave retardation plate to determine the ordering configuration within LC phase. The schematic illustration of experimental system and the optical responses and schematics of LC phases when in contact with non-surfactant and surfactant solutions can be seen in Figure 2.5. They carried out experiments to evaluate the sensitivity, stability and reusability of their developed system and found out that this microcapillary-based optical sensor was stable for 120 h long and could be used at least 10 times without the sensitivity loss. Also, they observed that their microcapillary-based sensor is more sensitive than LC-solid interface counterparts.

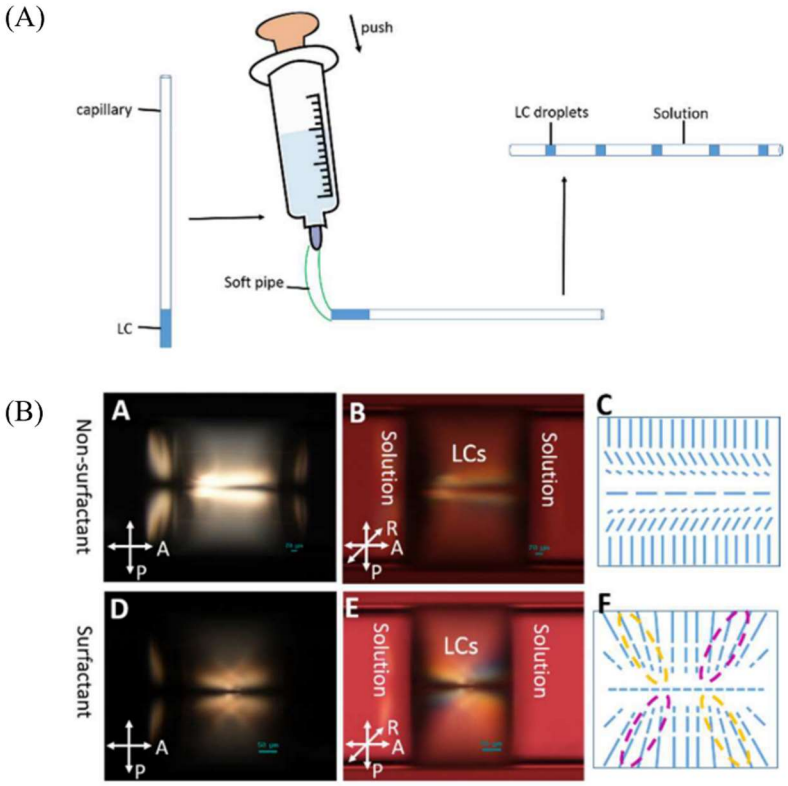

Figure 2.5 (A) Schematic representation of microcapillary-based experimental system, (B) Optical images (A-B and D-E) and schematic illustrations (C and F) of LC contacting with non-surfactant and surfactant solutions. Left columns belong to the polarized optical images while middle columns belong to the full wave retardation plate. [51]

More recently, Nguyen et al. developed a microcapillary-based biosensor for the detection of pesticides.[7] They used several mixtures of acetylcholinesterase (AChE), myristoylcholine chloride (Myr), and fenobucarb and malathion as pesticides to observe the response of the system. By treating the inner walls of microcapillaries with OTS, they give homeotropic alignment to LC mesogens on the glass surface. With the formation of Myr, a cationic surfactant, monolayer at the LC-aqueous interface, four-petal appearance was observed since LC assume homeotropic orientation when in contact with Myr. When the AChE meets the Myr molecules, hydrolysis takes place, choline and myristic acid are formed which disrupts the Myr monolayer at the interface. As a result, orientation transition from homeotropic to planar was observed at LC-aqueous interface. However, since the pesticides inhibit

the activity of AChE enzyme, when fenobucarb and malathion were present in the aqueous solution, LC orientation remains homeotropic at the aqueous interface which again leads to the four-petal appearance within LC compartment. The detection limits were reported as 5 pg/mL and 2.5 pg/mL for fenobucarb and malathion, respectively. Schematic illustration and the optical micrographs for the system was given below in Figure 2.6.

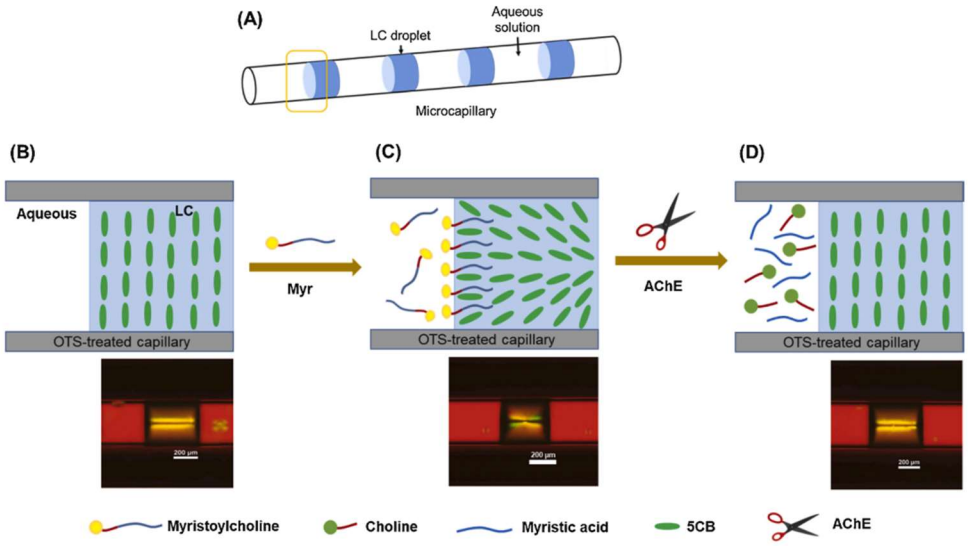

Figure 2.6 Schematic illustration of LC-based sensor for the detection of pesticides in aqueous environment. (A) Preparation of LC compartments within OTS-treated microcapillary. Schematic representation (top) and optical micrographs (bottom) of LC compartments contacting with (B) pure PBS solution (pH=7.4), (C) Myr aqueous solution, and (D) a mixed solution of Myr and AChE. [7]

The proposed microcapillary-based sensors in past examples are promising.[7,9,50,51] However, these past examples do not offer a control over the LC compartment sizes, the LC-solution interface, and do not offer free interfaces for species exchange. Also, although the initial and final configurations and characterizations were given in these studies, there is limited information provided for transition states. However, recent studies have shown that the time-dependent information of LC ordering transitions to gain importance.[30–32,52] Şengül et al. investigated the LC droplet configurations which are induced by the adsorption of nanoparticles.[32] They used 100 nm-in-diameter silica nanoparticles whose surfaces were functionalized with either

DMOAP or DMOAP/COOH mixed monolayer to promote either homeotropic or planar LC anchoring, respectively. They showed that the adsorption of surface-functionalized nanoparticles depends on the pH of the system and the nanoparticle concentration. Also, they highlighted the time-dependent configuration distribution of LC droplets as they were incubated in DMOAP/COOH mixed-monolayer-coated nanoparticles at pH=5.9, whereas they did not observe this behavior at pH=3 as can be seen in Figure 2.7. They stated that one can get the information of the physicochemical properties of the nanoparticles based upon the configuration distributions in the means of hydrophobicity or the surface charges of the particles.

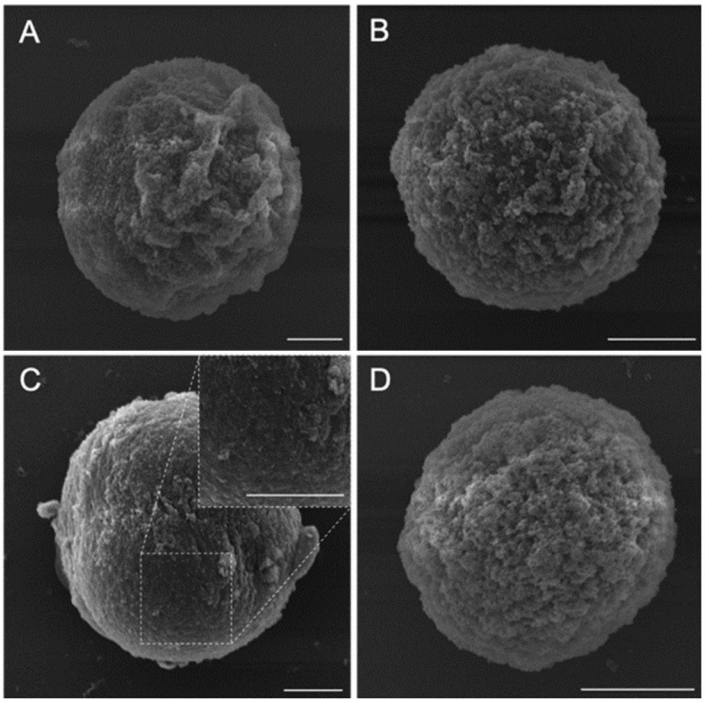

Figure 2.7 Scanning electron micrographs of the polymerized LC droplets after contacting with suspensions of silica nanoparticles functionalized with mixed monolayers of COOH-terminated silanes and DMOAP at (A, B) pH=3, and (C, D) pH=5.9. The images were collected from polymerized droplets of 25 %wt RM257/5CB mixture after equilibration for (A, C) 10 mins, and (B, D) 90 mins in the suspensions. Inset in (C) shows the magnified image of the are indicated by dashed lines. Scale bars: 5 μm. [32]

Such studies showed that with proper image processing and machine learning algorithms, rapid identification of species can be achieved with the use of the

transition state configurations that were triggered by the changes in surface anchoring.[30,31,52] For this purpose, Smith et al. proposed a LC-based sensor which automatically discriminates the species based on the spatial optical responses of LCs when exposed to different chemical environments.[30] By training VGG16 convolutional neural network (CNN) with predetermined features obtained from color micrographs, they acquired excellent classification accuracy between dimethyl methylphosphonate (DMMP) and humid nitrogen although LC mesogens respond similarly when they are exposed to these chemicals. Even though the final response of the LC-based sensor show similarity, they were able to differentiate the species with the information of transition states of the first 30 seconds since the optical responses of DMMP and humid nitrogen differs spatially (see Figure 2.8) which reduces the detection times.

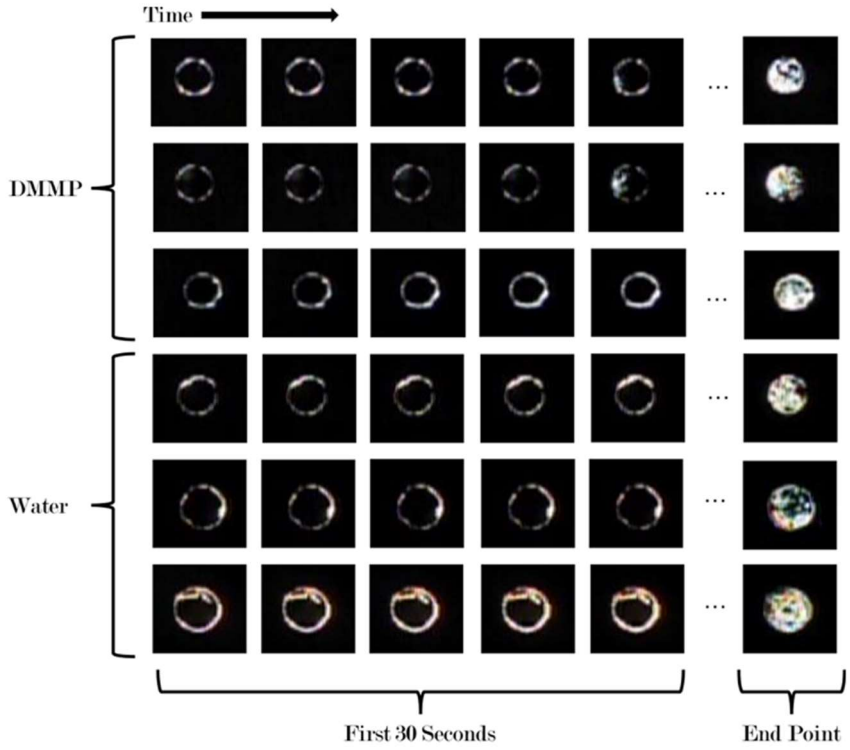

Figure 2.8 Optical responses of LCs under gaseous N_2-water (30% relative humidity) and N_2-DMMP (10 ppm) environments at room temperature. [30]

Herein, we seek to develop a portable and affordable microcapillary-based sensing system that can be used for the online detection and characterization of chemical and

biological species in different environments. The proposed system also allows acquisition of the information from the transition states which is triggered by the adsorption of analytes on LC-aqueous interfaces. Based on these, the outcomes of this thesis can be for the benefit of future researches to enhance the LC-based sensors for the detection of biological and chemical species, where LC is confined in microcapillaries.

CHAPTER 3

MATERIALS AND EXPERIMENTAL SECTION

3.1 Materials

Nematic LC 4-cyano-4'-pentylbiphenyl (5CB) was purchased from HCCH Jiangsu Hecheng Chemical Materials Co. Ltd. (Nanjing, China). Sodium dodecyl sulfate (SDS), dimethyl octadecyl [3-(trimethoxysilyl) propyl] ammonium chloride (DMOAP), (3-Aminopropyl)triethoxysilane (APTES), glutaraldehyde (GA) solution, sulfuric acid, hydrogen peroxide solution, glycine, phosphate buffered saline (PBS), neomycin B, ampicillin and hexadecyltrimethylammonium bromide (CTAB) were obtained from Sigma-Aldrich (St. Louis). The DNA aptamer (/5AmMC6/GGG AGA CAA GGA AAA TCC TTC AAT GAA GTG GGT CGA CA) and RNA aptamer (/5AmMC6/GGC UGC UUG UCC UUU AAU GGU CCA GUC) used in the experiments were synthesized by Integrated DNA Technologies. Glass microcapillaries with diameter of ~700 μm were purchased from Drummond Scientific Company (Broomall, PA, USA). Anhydrous ethanol was purchased from Isolab (Eschau, Germany). TEM Grids were obtained from EMS (Hatfield, PA). Glass slides were obtained from Marienfeld GmbH (Lauda-Königshofen, Germany). The ultra-pure water with a resistivity of 18.2 MΩ.cm is used.

3.2 Microcapillary-Based Optical Sensor

3.2.1 Preparation of Aqueous SDS Solutions

Aqueous SDS solutions with various concentrations (0.05 - 50 mM) were prepared by using water. Serial dilution was done for lower concentrations.

3.2.2 Functionalization of Glass Microcapillaries and Glass Slides

Glass microcapillaries and glass slides were immersed in aqueous DMOAP solution to form self-assembled monolayers (SAMs) with covalent binding of silane groups to the glass surfaces and sonicated at room temperature for 10 min. Then, they were rinsed with excess water, and dried under stream of N_2

3.2.3 Preparation of Microcapillaries Confining the LC and Aqueous Media – This Thesis

On a clean glass slide, two separate drops of 0.5 μL SDS solution with a known concentration, two separate drops of 1.5 μL water and a small droplet of 5CB were prepared. Fluids were drawn into the DMOAP-coated glass microcapillary with the wiretrol in the order of SDS solution-water-5CB-water-SDS solution. After injection of each solution compartments, we pushed the liquid slowly out to obtain a convex curvature at the end of the capillary which will be in contact with the next solution of interest to avoid air bubbles (See Figure 4.1 for the illustration of the experimental setup). SDS solutions were diluted by 4 times during the experiment since the ratio of SDS solution/water is 1:3 unless otherwise stated.

3.2.4 Preparation of Microcapillaries Confining the LC and Aqueous Media – Literature

On a clean glass slide, 3 μL SDS solution with a desired concentration (concentration of prepared SDS solutions ranged between 0.0125 - 12.5 mM for this method) and a small droplet of 5CB were prepared. By touching, 5CB was siphoned inside the DMOAP-treated 5 μL volume glass microcapillary. Then, with a plunger, SDS solution was syringed inside the microcapillary which divided the 5CB into compartment with different sizes.

3.2.5 Preparation of Optical Cells

20 μm-thick gold TEM grids were placed on the surface of DMOAP-treated glass slides. Grids were filled with approximately 1 μL of nematic 5CB, where excess 5CB was removed with a syringe. Glass slides with the filled gold grid were incubated in 1.2 mL water at room temperature for optical characterization. 0.4 mL of SDS solutions with varying concentrations were dropped on the optical cells to satisfy the desired ratio of SDS solution/water (1:3) for the experiments.

3.2.6 Preparation of LC Droplets in Aqueous SDS Solution

SDS solutions with varying concentrations (0.05 - 50 mM) were prepared, then diluted with water to satisfy the 1:3 volume ratio of SDS solution/water for the experiments. 1 mL of each solution was mixed with approximately 3 μL of nematic 5CB in the vial. The vial then was stirred for 10 seconds to form the LC droplets dispersed in the aqueous media.

3.2.7 Optical Characterization of LC Textures inside Microcapillaries and on Flat Films

Optical characterization of LC textures for the microcapillaries and flat films were performed by using Olympus BX53 microscope (Japan) equipped with crossed polarizers and U-TP530 full-wave retardation plate. Images were taken with 4x objective.

3.2.8 Optical Characterization of LC Droplets

Optical characterization of LC textures for the droplets were performed by using Olympus BX50 microscope (Japan) equipped with polarizer and analyzer.

3.2.9 LC Compartment Size Measurements

Analysis of the size of the LC compartments and the location of the defects were done by using Fiji ImageJ, which is an open source image analysis software.

3.2.10 LC Tilt Angle Measurements

LC maintained in TEM grids were prepared according to the procedure given above and placed under polarized optical microscope. For each SDS concentration, local uniform dark regions within grids were scanned. When dark regions were spotted, the plate was rotated 45° clockwise. Then, Olympus U-CTB Thick Berek Compensator was inserted which is initially set to 30°. The compensator knob was rotated clockwise until the observation of the first black line passing through the sample. The angle reading from the compensator was noted as θ_1. Then, the compensator was set to 30° again and the same procedure was carried out in counterclockwise direction. This value was noted as θ_2. For each SDS concentration, this procedure was repeated for 5 times. From these values, $\theta = |\theta_1 - \theta_2|/2$ angles were calculated and then, from the optical retardance values which is provided with the compensator as a function of θ angles, tilt angles were obtained.

3.3 Aptasensor

3.3.1 Cleaning of Glass Surfaces

Firstly, glass slides were cut into size of 2 cm x 6 cm rectangle. Then, glass slides and microcapillaries were immersed in a freshly prepared piranha solution (70% H_2SO_4 and 30% H_2O_2, v/v) at 80 °C for 2 h and 5 h, respectively to remove all organic contaminants and create hydroxyl groups on the glass surface. The cleaned glass surfaces were rinsed with water, ethanol, dried under stream of N_2 gas and placed in the oven at 110 °C for 1 h prior to functionalization.

3.3.2 DMOAP Functionalization

Glass slides were immersed in aqueous DMOAP solution and sonicated at room temperature for 15 min. Then, they were rinsed with excess amount of water, dried under stream of N_2.

3.3.3 APTES/DMOAP Functionalization

Aqueous solution containing 10% (v/v) APTES and 1% DMOAP (v/v) were stirred at 80 °C for 30 min prior to functionalization. Then, glass slides and microcapillaries were immersed in the solution for 1 h at 80 °C to bind the glass surface with covalent bonding between silane groups of the APTES/DMOAP and hydroxyl groups on the glass surfaces. They were rinsed with copious amount of water, dried under stream of N_2, stored in an oven at 110 °C for 1 h for use.

3.3.4 Aptamer Immobilization

APTES/DMOAP functionalized glass surfaces were immersed in 1% (v/v) GA aqueous solution for 30 min at room temperature to bind GA molecules covalently to APTES molecules. They were rinsed with excess water, dried under stream of N_2. For both RNA and DNA aptamer which will be used for the detection of neomycin B, aptamer was dissolved in PBS to obtain 1 μM solution for glass slides and 500 nM solution for microcapillaries.[53] 5 drops of aptamer solution(5 μL for each droplet) were dropped on the glass slides at specific places; while glass microcapillaries were immersed in the freshly prepared aptamer solution. Immobilization took 4 h at room temperature. Then, glass surfaces were rinsed with PBS and water, dried under N_2. Subsequently, glass surfaces were immersed in 80 mM aqueous glycine solution for 1 h at room temperature to block the unreacted aldehyde groups, rinsed with water and dried under N_2.

3.3.5 Target Incubation

Target solutions (either neomycin B or neomycin B-ampicillin mixture, see Figure 3.1 for the structures) with various concentrations were prepared in PBS buffer. 80 μL of target solution were dropped on the glass slides at specific places for 30 min at room temperature. Glass microcapillaries were immersed in the target solution for 105 min at room temperature. Glass surfaces were rinsed with PBS and water, dried under N_2.

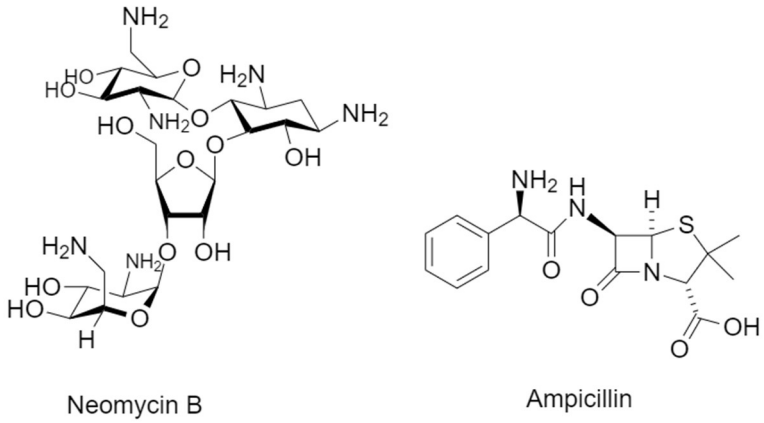

Figure 3.1 Chemical structures of neomycin B and ampicillin.

3.3.6 Preparation of LC Sandwich Cells

The optical cells were constructed by sandwiching LC between the two solid surfaces. DMOAP-functionalized glass slide was used as the bottom surface; while aptamer-immobilized glass slide was used as the top. 20 μm-thick spacers were used to separate the surfaces. Nematic 5CB was then filled in the sandwich cell by capillary action at room temperature.

3.3.7 Preparation of LC Optical Cells inside Microcapillaries

On a clean glass slide, 1 μL nematic 5CB was dropped. By the use of wiretrol, 5CB was siphoned inside and separate LC compartments (100 - 1000 μm-sized) were formed inside aptamer-immobilized glass microcapillaries.

3.3.8 Optical Characterization of LC Textures inside Microcapillaries and on Flat Films

Optical characterization of LC textures for the microcapillaries and flat films were performed by using Olympus BX53 microscope (Japan) equipped with crossed polarizers and U-TP530 full-wave retardation plate. Images were taken with 4x and 50x objectives. Mean grayscale measurements were done by using Fiji ImageJ.

CHAPTER 4

RESULTS AND DISCUSSION

In this thesis, we proposed two portable microcapillary-based LC sensor implementations. In the first part of the thesis study, we developed a sensing system that can be used for the online detection and characterization of chemical and biological species in aqueous medium, which also allow acquisition of the information from the transition states. In the second part, we designed a biosensing system where we used aptamers and LC-solid interactions for specific recognition purposes, whose pre-development studies were done with LCs sandwiched in flat surfaces.

4.1 Microcapillary-Based Optical Sensor

We use LC compartments with sizes of 700 μm-in-diameter and 300-1400 μm-in-length formed in glass microcapillaries. Schematic illustration of the system is given in Figure 4.1. Glass microcapillaries were treated with DMOAP to maintain homeotropic LC alignment. SDS solution with a specific concentration, water and nematic 5CB were initially filled into the capillary as sketched in Figure 4.1A. We kept the volume ratio of SDS solution to water as 1:3 unless otherwise indicated. As a result of the diffusion of SDS molecules through the water, same bulk solutions on both sides of the LC compartment were obtained in which SDS solution was diluted four times from its initial concentration (Figure 4.1B, C). For the rest of the study, we report the experimental data as the final SDS concentration in the aqueous phase.

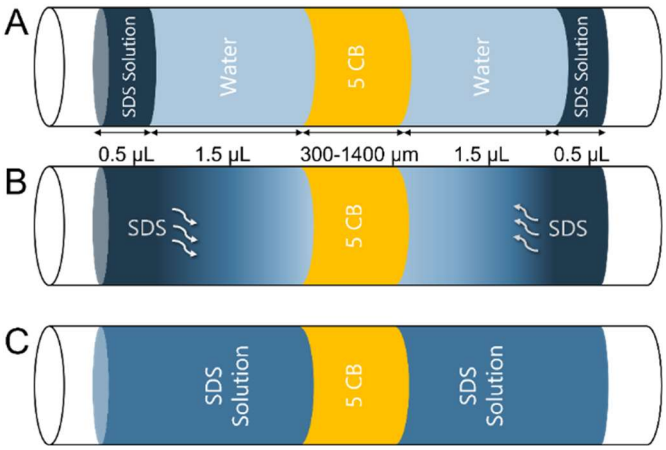

Figure 4.1 Schematic illustration of the experimental procedure followed in the study (A) initial, (B) intermediate, (C) final.

4.1.1 Characterizations of the System Configurations

In Figure 4.2 below, we illustrated the optical appearance of the LC maintained initially when in contact with an aqueous interface, the transition and equilibrium states maintained in LC compartment upon contact with aqueous SDS solutions (see also Figure 4.3). In Figure 4.2A, we obtained LC-aqueous interface in which LC exhibits planar anchoring consistent with the literature.[17,54] Homeotropic LC anchoring at the inner capillary interface was maintained due to DMOAP functionalization.[55,56] A characteristic dark brush at the center of the capillary between two bright horizontal domains, and a point defect formed at the vicinity of the LC-aqueous interfaces resulting from the combination of homeotropic and planar alignment at the glass and LC-water interface, respectively, was observed during experiments. When the capillaries were imaged under the retardation plates, the observed blue and orange color hue above and below the bright domains (respectively) are the indicatives of parallel and orthogonal alignment of the mesogens with respect to the alignment of the retardation plates. Under these conditions, the LC configuration is consistent with the escaped radial configuration as reported in the literature and as sketched in Figure 4.2(right).[51,57–60] Here we note that we have performed the filling of the compartment from right to left side in

reference to Figure 4.2A, and we observed up to 85% of the compartments to maintain the configuration with the same symmetry, a positively charged defect at the right side, a negatively charged defect at the left side, as shown in the figure. The rest 15% of the compartments were the mirror image of this configuration. We hypothesized that the symmetry was due to the shear induced in the compartment due to the filling.

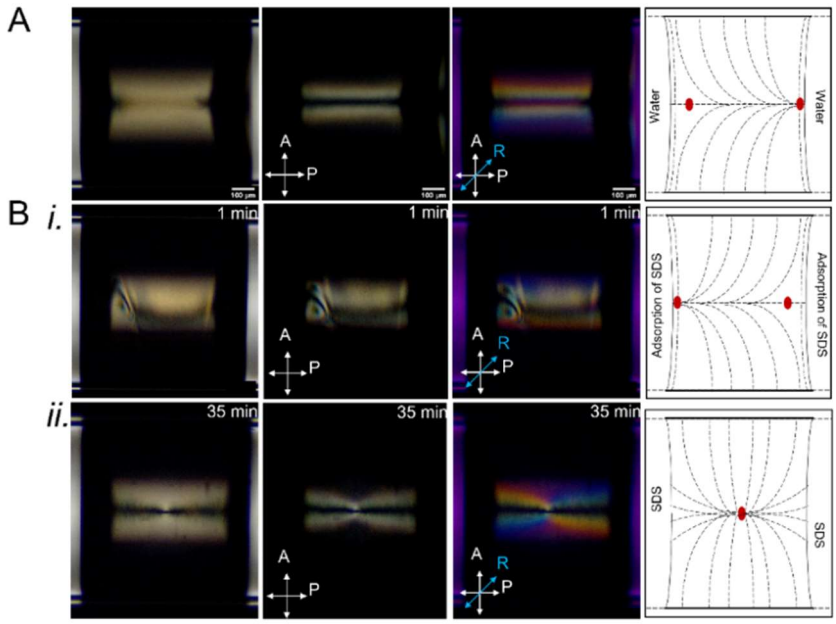

Figure 4.2 Micrographs of nematic 5CB compartments confined to DMOAP-treated microcapillaries collected in brightfield (first panel), under polarized light (second panel) and with retardation plates (third panel). (A) The configuration of nematic 5CB compartment when in contact with water, (B) transition configuration of nematic 5CB when contacting with 1.25 mM SDS solution, at t=1 min (C) equilibrium (final) configuration of nematic 5CB, contacting with 1.25 mM SDS solution, at t=35 min. Arrows labelled A and P indicate the directions of the analyzer and the polarizer, respectively. R indicate the axis of the retardation plate. Schematic illustrations of the corresponding configurations of nematic 5CB compartments are shown in the rightmost panel. Red dots and dashed lines represent defects and alignment of LC mesogens. Scale bars: 100 μm.

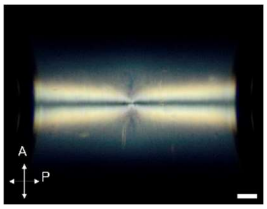

Figure 4.3 Equilibrium configuration of LC compartment inside microcapillary with high exposure time to observe dark vertical and horizontal lines crossing through the point defect. Scale bar: 100 μm.

When the compartments were contacted with aqueous SDS solutions, after the diffusion followed by the adsorption of SDS molecules at the LC-aqueous interface, we observed a transition from planar to homeotropic orientation at the LC-aqueous interface. This resulted in an equilibrium configuration shown in Figure 4.2B-*ii* with a four-petal appearance under polarized light. The blue and orange color hue at the two poles of the four-petal appearance was observed under POM equipped with a retardation plate and the defect at the center of the LC-compartment were evidently the indicatives of the LC director profile schematically shown in Figure 4.2B-*ii* (right). We can conclude that, the two distinct optical appearance shown in Figure 4.2A and B-*ii* are the results of the different anchoring conditions at the two LC-water interfaces, consistent with the past examples.[51]

A transient configuration is present between the escaped radial and four-petal configurations as shown in Figure 4.2B-*i*, which was collected after 1 min of incubation of LC compartment in aqueous SDS solution. As shown, a point defect at the left side of the compartment that corresponded to the side with a positively charged defect as sketched in the right panel. We observed this transient state to take 41 ± 19 min to equilibrate and form the final, four-petal configuration. This observation showed that reaching the equilibrium configuration was not that rapid to achieve the desired response time. Thus, we further investigated the origin of this transition. First, we estimated the time for the diffusion process in the scales of minutes together with the experiments that we performed with 5CB placed in TEM grids, consistent with the literature.[17] We have also performed the experiments with different geometries using the same capillary-based system for the diffusion of SDS

molecules. The volumes of the aqueous SDS solution and water were doubled preserving the 1:3 ratio of SDS solution/water to see the effect of the diffusion path length of SDS molecules (Figure 4.4). With doubling the path length, we did not observe a significant change in the time required to reach equilibrium four-petal configuration, supporting the fast diffusion process compared to the ordering transition.

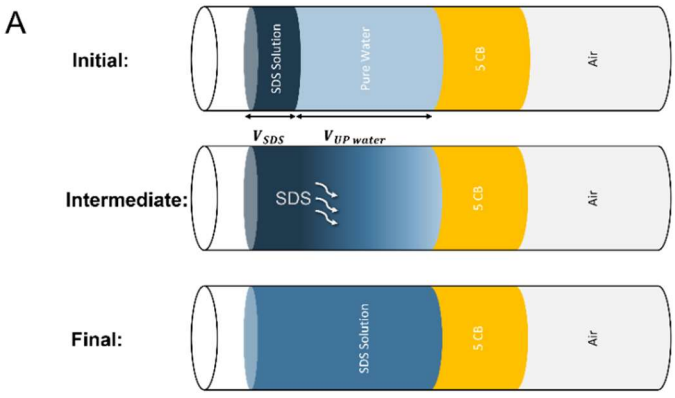

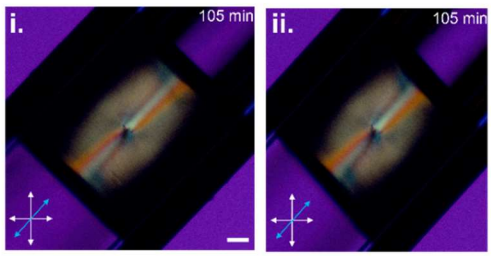

C

$V_{SDS}/V_{UP\ water}$	0.5 µL/1.5 µL		1.0 µL/3.0 µL	
	t (min)	d (µm)	t (min)	d (µm)
Equilibrium	40	1650	225	1226
	20	1180	60	618
	50	1138	165	1080
	235	1468	55	558
	105	834	105	756
	245	1454	75	539
Average	**115.8**	**1287**	**114.2**	**796**

Figure 4.4 Diffusion and equilibrium time analysis with the systems where one side of the LC phase was opened to atmosphere; (A) Schematic representation of experimental setup, (B) 45 ° angled POM images of LC compartments where aqueous SDS solution/UP water volumes were (i.) 0.5 µL/1.5 µL and (ii.) 1.0 µL/3.0 µL. (C) Equilibrium times for each volume ratios, d represents the LC compartment size. Scale bar: 100 µm.

During the transition from the escaped radial to the four-petal configuration, we observed a continuous motion of the defect inside the capillary until it reached equilibrium. The micrographs collected during motion are shown in Figure 4.5A. The motion of the defect from the interface to the center of the LC compartment let us monitor the time-dependent ordering transition. Figure 4.5A shows the division of the distance of the defect from the LC-aqueous interface (l_0) by half length of the LC compartment (L). The logarithmic decay in the velocity (Figure 4.5B inset) of the defect with time was evident in the plot as the defect approaches the center of the compartment (l_0/L=1). This observation is consistent with the motion of the defect that results from the imbalances of the forces exerted on the defect as reported in the literature, where elastic forces, the forces resulting from reorientation and viscous drag force to result in the logarithmic decay of the distance to the center of the LC compartment was shown.[61] Thus, the measured times for the transient state to reach equilibrium was associated to the motion of the defects due to the imbalance in the elastic forces within the capillary that was formed after the anchoring transition upon adsorption of the SDS molecules to the LC-water interface. Consistently, we observed a slower transition to the final equilibrium state when the LC compartment was contacted with lower concentration of surfactants, highlighting the role of the surface anchoring and elastic forces on the motion of the defects (Figure 4.5). Therefore, the onset of the motion of the defects, which was measured to be observed within ~1 min could be considered as the sensor response.

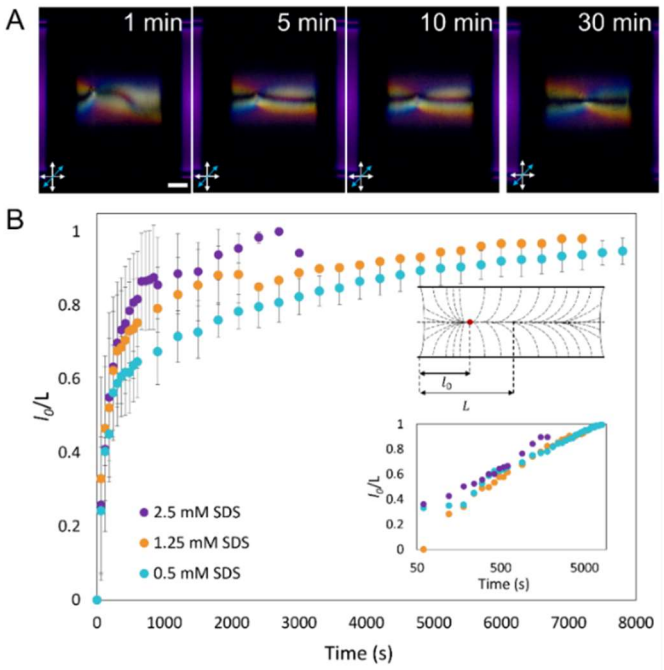

Figure 4.5 (A) Images of nematic 5CB confined to DMOAP-treated capillary in contact with 2.5 mM SDS solution at t=1 min, 5 min, 10 min and 30 min with full-wave retardation plate inserted. Scale bar: 100 µm. (B) Graphical representation of location of the defect with respect to time for LC compartments contacted with either 0.5, 1.25, or 2.5 mM SDS solutions. Inset shows the plot in the logarithmic time scale. $l_0/L=0$ represents the LC-aqueous interface, whereas $l_0/L=1$ indicates the center of the LC compartment.

In addition to the motion of the defects, in some of our experiments, we observed metastable states that persist in considerable times. To check this metastability, we increased the temperature above nematic-isotropic phase transition temperature of 5CB (35°C) to observe the change in the ordering of LC in compartment. After 5CB was cooled to room temperature nematic phase again, we observed the four-petal appearance (Figure 4.6). Obtaining the four-petal appearance after clearing the transition history with the sudden changes within the system temperature showed that although the surface anchoring transition from planar to homeotropic occurred at the LC-water interfaces, the system may also maintain metastable configurations. In addition, we also found that the frequency of the metastable states to be independent of the compartment size within the range that we study.

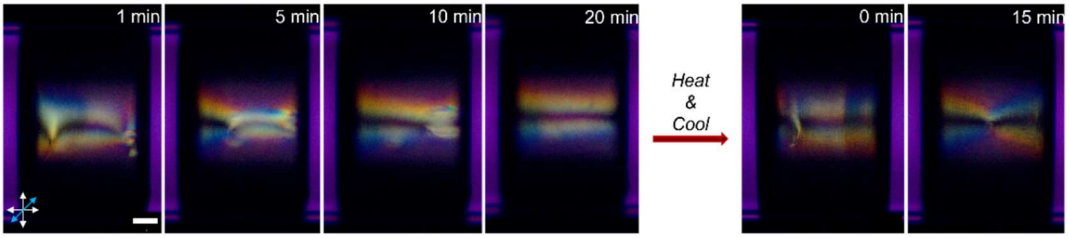

Figure 4.6 Optical images of time-dependent ordering transition of nematic 5CB confined to DMOAP-treated capillary in contact with 2.5 mM SDS solution before heating up to nematic-isotropic phase transition temperature(left) and after cooling down to the room temperature(right). Scale bar: 100 μm.

4.1.2 Response of the Liquid Crystal Microcapillary-based Sensor

After performing characterizations of the system configurations at escaped radial, transition and four-petal states, we carried out the experiments with aqueous SDS solutions of varying concentrations (0.0125-12.5 mM) for the measurement of the response of the LC microcapillary-based sensor. The percentages of experiments which we observed four-petal appearance at equilibrium with respect to the final SDS concentration are given in Figure 4.7A. At the SDS concentrations of 0.5 mM and above, we observed four-petal appearance with percentages above 80%. Moreover, all the experiments conducted with 1.25 mM and above SDS solutions resulted in four-petal appearance at equilibrium. Although the percentages were much lower for SDS concentrations below 1.25 mM, we observed four-petal appearance in some of the experiments carried out with 0.125, 0.25 and 0.5 mM SDS concentration. For the experiments which four-petal appearance was observed at equilibrium with varying SDS concentrations, fractions indicating whether four-petal appearance was obtained at room temperature or after the heating to overcome the metastability are illustrated in Figure 4.7B. The results showed that, four-petal appearance was observed for SDS concentrations even lower than 1 mM which is the SDS concentration needed for the monolayer coverage at the LC-water interface.[54] Below this concentration, planar-tilted anchoring of LC is observed resulting from the partial coverage of the LC-aqueous interface with the surfactant molecules.[54] To confirm our hypothesis, we measured the tilt angle of the LCs at

their interfaces equilibrated with the aqueous solutions of SDS. The measurements, consistent with the literature values, are given in Fig. 4A which showed that the tilt angle measurements were correlated with the response measurements collected with the LC microcapillaries.[54]

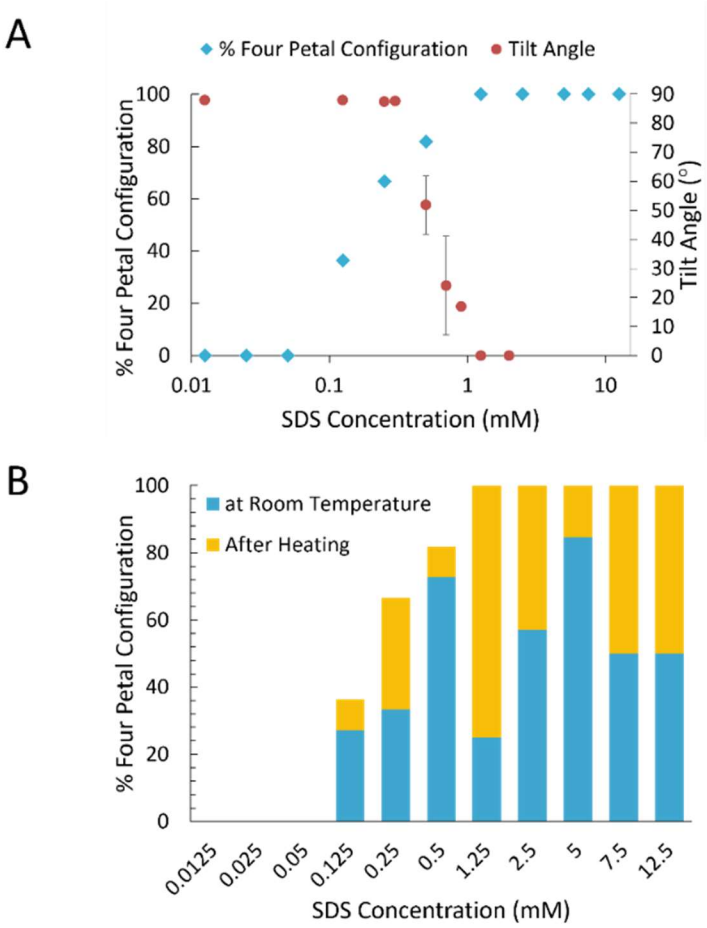

Figure 4.7 Distributions of (A) overall number of experiments that four petal configuration is observed (at room temperature and after heating in total) with various concentrations of SDS solution and the mean of the tilt angle at LC-water interface, (B) number of experiments that four petal shape is observed whether equilibrium was achieved at room temperature or after increasing the temperature to nematic-isotropic phase transition temperature with various concentrations of SDS solution.

We also note here that we have performed similar analysis with aqueous solutions of hexadecyltrimethylammonium bromide (CTAB) and obtained similar results (Figure 4.8).

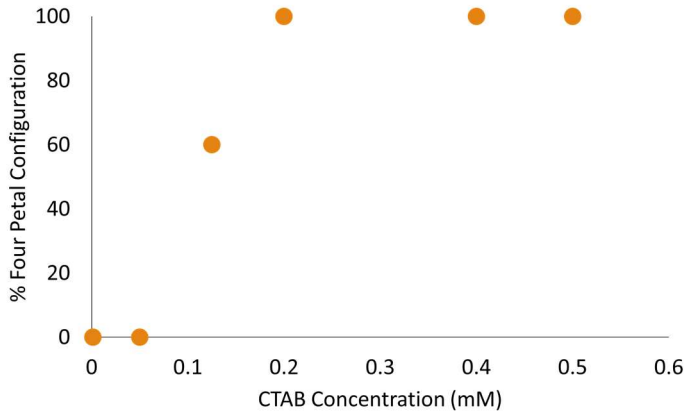

Figure 4.8 Distribution of overall number of experiments that four petal shape is observed with various concentrations of CTAB solution.

We next carried out experiments to compare the response of our sensors with their counterparts in the literature where LC (*i*) was on flat solid glass film within TEM grids, (*ii*) as droplets dispersed in water, (*iii*) confined in microcapillary with the method proposed in the literature[51], (*iv*) confined in microcapillary with our method. In flat systems, characterization of planar-to-homeotropic orientation transition is carried out by observing the changes in the color appearance from bright to dark (Figure 4.9A). Total darkness implies that the orientation at that interface is uniformly homeotropic. However, during transition from bright to dark upon increasing SDS concentrations tilt of LCs at their interfaces results in a continuous change in coloring. In the method where droplets dispersed in fluid media, bipolar-to-radial configuration change indicates that the planar-to-homeotropic orientation transition occurred within the LC droplet (Figure 4.9B). Intermediate to these two configurations, different equilibrium states (such as axial, escaped radial or preradial) resulting from the tilted surface anchoring at the aqueous interface were also observed.[48] As seen from the optical images given in the Figure 4.9 below, sensitivity of the microcapillary-based methods is comparable with the sensing methods where flat films or LC droplets were used.

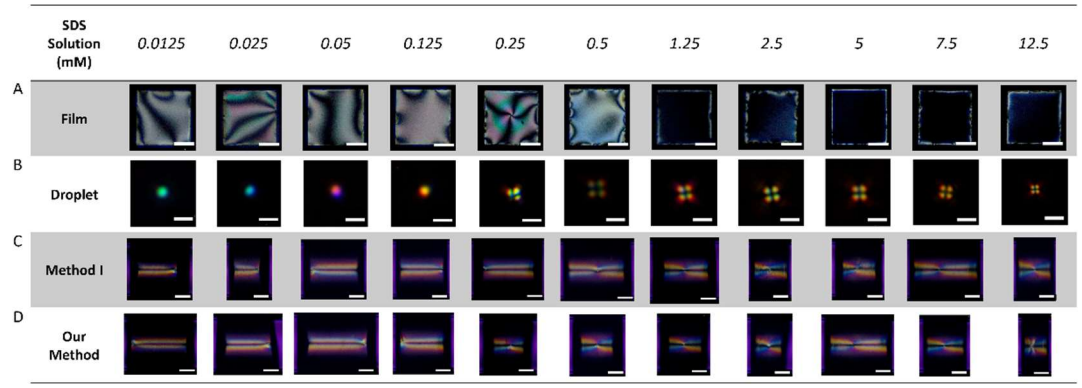

Figure 4.9 Optical images of nematic 5CB contacting with aqueous SDS solutions with varying concentrations from 0.00125 mM to 12.5 mM after dilution; (A) on flat glass film with TEM grids, (B) as droplets dispersed in water, (C) in microcapillary, LC confinement method proposed in somewhere else[51], (D) in microcapillary, our LC confinement method. For A, scale bars: 100 μm. For B, scale bars: 5 μm. For C and D, scale bars: 200 μm.

In addition to these, we make several observations that bring advantages to the microcapillary-based sensors we use. First, the LC compartment-based sensors provide binary response (planar appearance to four-petal appearance) with the distribution that can be correlated to the surface tilting. Thus, no additional measurements are needed (such as colorimetric measurements or use of compensators) for such quantification. Second, the binary response of the microcapillary-based methods also provides information about the surface concentration of the analytical species. Third, the quantification of the LC microcapillary-based methods is significantly easier than the LC sensors in films or droplet forms that could be collected with a regular camera (Figure 4.10). Lastly, LC compartment-based method that we propose herein would also provide means for portable, reversible, and wearable sensors due to their stable and robust form. In addition, LC microcapillary-based sensors provide interfaces that allow controlled exchange of the analytical species with the contacting aqueous phases.

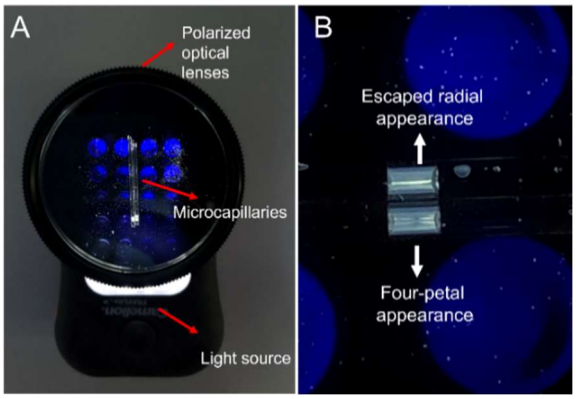

Figure 4.10 Real-time imaging of the microcapillary-based method; (A) Apparatus that is used for imaging, (B) LC configurations observed by using the apparatus.

4.1.3 Reversibility of the Liquid Crystal Microcapillary-based Sensor

We performed additional set of experiments to demonstrate the reversibility of the LC capillary-based sensors. For this purpose, we used the same experimental procedure described in Figure 4.1 to maintain four-peal configuration as the initial state. After we observed the four-petal appearance upon contacting the LC phase with 1.25 mM SDS solution (that causes homeotropic anchoring at the LC-water interface) as shown in Figure 4.11A, we equilibrated the aqueous phase at both ends of the capillary with copious amount of pure water (~100 mL). This process was planned in motivation to dilute the SDS solution in contact with the LC phase to a concentration such that the ordering transition from four-petal configuration to escaped radial configuration occurs. The resulting appearance of the LC compartment maintained in the microcapillary is shown in Figure 4.11B. Consistent with our expectation, dilution of the SDS solution in contact with the LC compartment resulted in the configuration transition to escaped radial indicative of the planar anchoring at the LC-water interface. Therefore, in the light of these results, we confirmed the reversibility of our sensor.

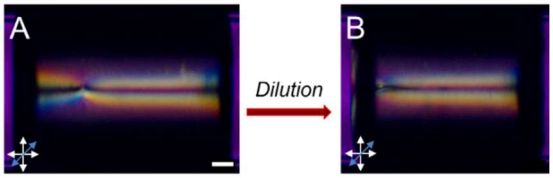

Figure 4.11 Polarized optical micrographs of nematic 5CB contacting with (A) aqueous 1.25 mM SDS solution at both sides of the LC compartment, (B) after dilution of the aqueous phase at both sides of the LC compartment. Scale bar: 100 μm.

When contacting the aqueous phase with pure water for dilution, the LC compartments within the capillary was moved. The surface tension at LC-water interface is reduced due to the presence of the SDS.[62] This reduction makes the dilution process shown in Figure 4.11 challenging. Such that, during the motion of the LC compartment within the capillary, we observed three kinds of processes happening. First, as seen in Figure 4.11, the LC compartment preserve its size and shape after the dilution process, at the end of which the escaped radial appearance is maintained. However, in some cases we observed breaking of the compartment that was initially maintained in the microcapillary, one example of which is shown in Figure 4.12B as the second case. As shown, the breaking of the LC compartment from its initial state (Figure 4.12A) resulted in the formation of discontinuous droplets positioned at the inner surfaces of the microcapillaries. With this, the compartment size was reduced, however, maintaining the final escaped radial configuration consistent with the planar anchoring at the two sides of the capillary. Third, the breaking of the compartment resulted in formation of two separate, smaller compartments as shown in Figure 4.12C. In this case, we observed the compartments to maintain appearances of either the four-petal or the escaped radial configurations that are stable at least over a day.

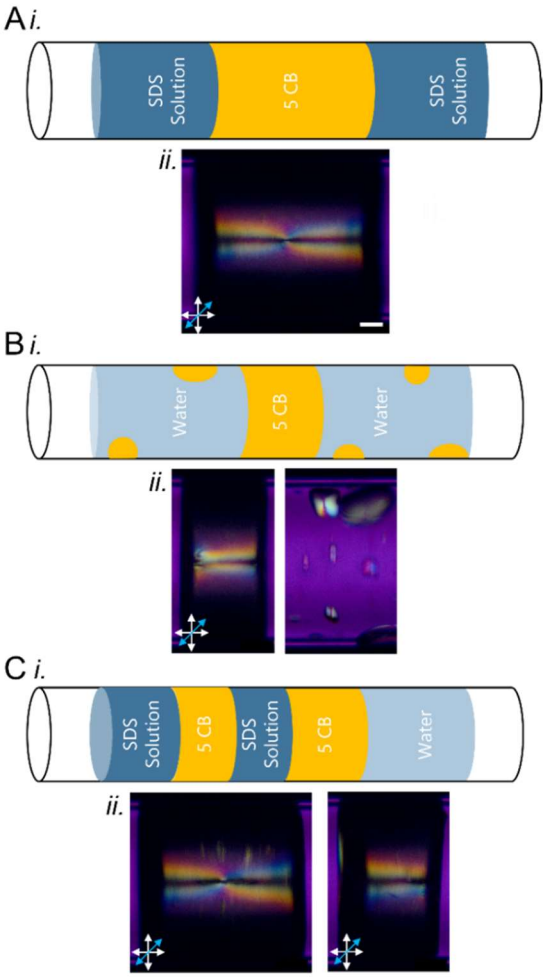

Figure 4.12 (A) Schematic representation (i.) and POM images (ii.) of the initial step of reversibility experiments prior to purification process; LC is contacting with 1.25 mM aqueous SDS solution at both sides, (B) i. Schematic representation of the first consequence of the purification process; LC droplets stuck on the glass capillary surface, ii. Optical images of the nematic 5CB for the first consequence of the purification process; first frame belongs to the equilibrium state when both sides of the LC compartment contacting with water, second frame belongs to the LC droplets stuck on the capillary surface, (C) i. Schematic representation of the second consequence of the purification process; LC compartment broke into multiple compartments, ii. Optical images of the nematic 5CB for the second consequence of the purification process; first frame belongs to the equilibrium state when the first LC compartment contacting with aqueous SDS solution at both sides and second LC compartment contacting with water at one side and aqueous SDS solution at opposite side. Scale bar: 100 μm.

As control experiments to this observation, we conducted new experiments where we (*i*) first, filled the microcapillary in the sequence: aqueous SDS solution-LC-

water, (*ii*) second, introduce SDS solution to water-end of the capillary to have the same SDS concentration at the both sides of the LC compartment to observe the four-petal appearance at equilibrium, and (*iii*) third, contacted the aqueous phase with copious amount of water for overnight to purify only one side of the LC compartment (Figure 4.13). When only one side of the LC compartment was aqueous SDS solution, we obtained an LC configuration with escaped radial appearance. After introducing SDS solution to the water-end of the capillary, we obtained four-petal appearance at equilibrium. After dilution of the one side, escaped radial appearance was maintained again. Thus, we concluded that the two configurations that we observe in the condition illustrated in Figure 4.12 was due to the partial compartmentalization of the SDS solutions between the LC compartments. As shown in the sketches, the LC compartments that are in contact with the SDS solutions maintained their four-petal appearance whereas their pure water contacting counterparts appeared escaped radial.

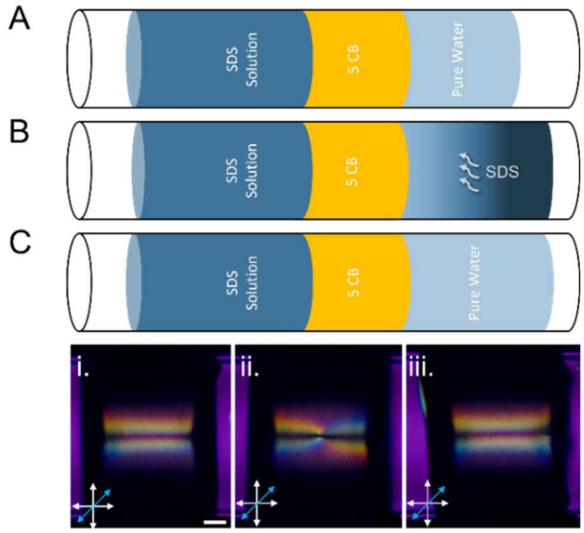

Figure 4.13 Schematic representations (A,B,C) and POM images (i, ii, iii) of (A, i) the initial step of the control experiments prior to purification process, LC compartment contacting with 1.25 mM aqueous SDS solution at one side and UP water on the other side, (B, ii) the equilibrium state when the both sides of the LC compartment contacting with 1.25 mM aqueous SDS solution, (C, iii) the equilibrium state when the LC compartment contacting with UP water at one side and 1.25 mM aqueous SDS solution at the other side again, after purification process. Scale bar: 100 μm.

Lastly, we also checked whether or not SDS can diffuse through LC compartment and eventually concentrated at the LC-water interface of the opposite side. For this purpose, we modified the arrangement shown in Figure 4.1 such that two LC and two aqueous phase compartments exist. Between the two LC compartments, we maintained water to mediate planar anchoring at the two LC-water interfaces. The remaining side of one of the LC compartments was left open to air, which mediate strong homeotropic anchoring, whereas the remaining side of the second LC compartment was contacted with SDS solution. (Figure 4.14). We did not observe the four-petal appearance in neither of the LC compartments. There was no change in the configuration of the LC even after we left it for one day at room temperature. Based on these results we can conclude that the solubility and diffusion of the SDS molecules are negligible and do not cause a significant change in neither of the LC-water interfaces.

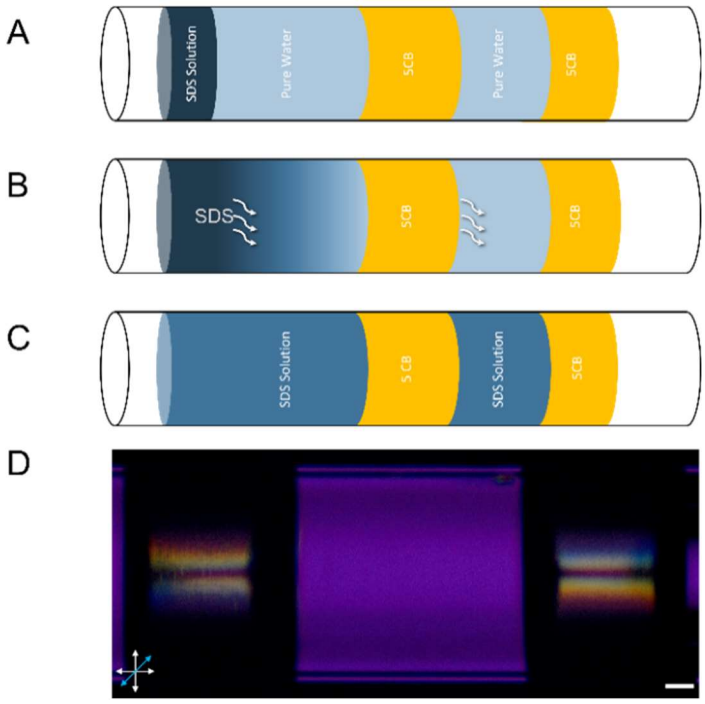

Figure 4.14 Experimental setup for the determination of SDS diffusion in LC phase: (A) initial, (B) intermediate, (C) final, and (D) POM images of both the LC compartments in final state. Scale bar: 100 µm.

4.2 Aptasensor

In the second part of this study, we developed aptasensors to be used in both flat and microcapillary geometries. In this strategy, we employed LCs to report the changes that occur at the solid interfaces. For this purpose, we first performed surface modifications and aptamer immobilization on flat glass slides. We optimized the concentrations of the solutions used for the surface modifications and conditions based on LC response after each surface functionalization steps. We determined the detection limit and commented on the selectivity of the aptasensing platform based on the known, flat systems.[1,5,6] Then, we adapted the followed procedure into microcapillaries to develop a portable and affordable biosensor providing easy quantification.

4.2.1 Aptasensor in Flat Sandwich Cells

We performed our preliminary biosensor studies in flat sandwich cells to provide a reference system, where we can characterize the detailed anchoring on the aptamer-immobilized surface.[1,5,6] For this purpose, we functionalized the bottom glass slides with 1% dimethyl octadecyl [3-(trimethoxysilyl) propyl] ammonium chloride (DMOAP) aqueous solution to make sure that we always maintain homeotropic anchoring at the bottom surfaces. Figure 4.15 shows the schematic illustration of the system used in this part of the study. We sequentially functionalized the upper surfaces of the flat sandwich cells with a mixture of (3-Aminopropyl)triethoxysilane (APTES)/DMOAP and then glutaraldehyde (GA) solution for immobilization of aptamers and target incubation. We placed five 5 μL droplets of aptamer solution to specific locations on the APTES-GA/DMOAP-functionalized glass slides as indicated in Figure 4.15A. To observe the LC-surface interactions on the same sandwich cell, we covered the three aptamer spots with 80 μL of target solutions whereas the rest of the two spots were not exposed to target molecules (Figure 4.15A). After aptamer immobilization step, we ensured LC to assume uniform

homeotropic anchoring which results in dark appearance under crossed polarizers (Figure 4.15B). When we exposed the three aptamer-immobilized spots to target solutions, aptamer bound to its target and formed "aptamer-target" complexes. Because of the these complexes, conformation of aptamer is changed which disturbs the LC orientation and we observed bright appearances indicating the orientation transition from homeotropic to planar (degenerate planar/tilted) (Figure 4.15C). As can be seen in Figure 4.15C-*ii*, we observed dark regions between bright spots which supported that orientation transition from homeotropic to degenerate planar/tilted was the result of aptamer-target bindings since these aptamer-free dark regions were also exposed to target solution. In addition, since we did not expose the right hand side of the glass slide having two aptamer-immobilized spots to target solution, we did not observe any response on that side of the sandwich cell. This is an important observation as the two aptamer-bound spots on the right side were exposed to rinsing and drying steps followed after target incubation step (Figure 4.15B-*ii*) which appearently did not alter its anchoring condition.

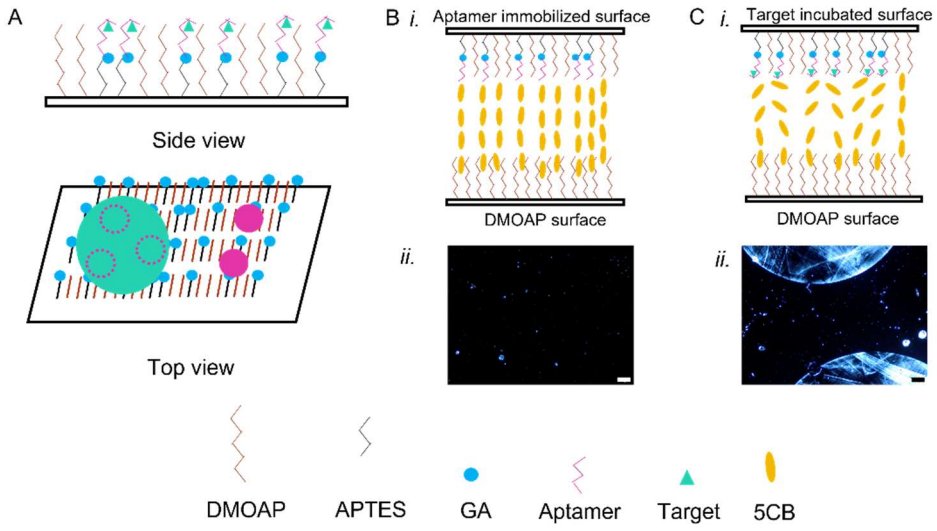

Figure 4.15 (A) Schematic illustration of the upper surface modified glass slides for aptasensing platform. (*i.)* Schematic representations, and *(ii*.) polarized optical micrographs of LC configuration in the optical cell (B) homeotropic orientation in the absence of target solution, and (C) degenerate planar/tilted orientation after incubation with target solution. Scale bars: 200 µm.

We carried out experiments to determine the optimum system and procedure conditions which we explained below. Polarized optical images that were given in Figure 4.15B, C were representative images which were taken during experiments after optimizations.

4.2.1.1 Surface Functionalization and Aptamer Immobilization on Glass Surfaces

We functionalized the upper glass surfaces with APTES/DMOAP mixed monolayers to provide both homeotropic alignment and reactive sites for further modifications. DMOAP is known to give homeotropic anchoring of 5CB due to long alkyl chains in its structure.[55,56] Also, APTES, which we observed to mediate planar LC anchoring, should be available in sufficent quantity on the surface since it offers amine groups for aptamer immobilization via GA linkage method.[1,63,64] Although the concentration of bulk APTES/DMOAP solutions which were prepared for the surface silanization was known, the concentration distribution on the surface might be different. The distributions of silane groups on the surfaces can be determined by using analytical methods like XPS, FTIR etc.; however, without the information of exact surface concentration, we could continue our experiments by using optical responses which were collected under crossed polarizers for varying ratios of APTES/DMOAP mixtures and sequential surface modifications.[65–68] Since we expected to observe bright appearances as the response of our sensor which is the indicative of planar/tilted orientation, we wanted to preserve the homeotropic anchoring of LC molecules until the end of aptamer immobilization stage. However, since LC alignment is affected by the interfacial composition of APTES/DMOAP, we conducted experiments with different APTES/DMOAP mixture ratios in reference to the literature and solvents to find the optimum condition.[1,5,6] As shown in Figure 4.16A-C, the higher APTES/DMOAP ratio of 20:1 (v/v)% resulted in bright images when imaged under POM indicating that LC alignment is planar on upper surface consistent with the literature (Figure 4.16E).[1,5,6] Also, although

aqueous solutions of 5:1 (v/v)% APTES/DMOAP mixtures led to completely dark background, we observed bright images under POM when 5:1 (v/v)% APTES/DMOAP mixtures prepared in absolute ethanol (Figure 4.16A, D). Despite both aqueous APTES/DMOAP solutions with ratios of 5:1 and 10:1 offer uniformly dark background, the subsequent experimental results of LC sensing cells formed with glass slides functionalized with 5:1 (v/v)% APTES/DMOAP aqueous mixtures were unsatisfactory. Based on these results, we carried out the consequent experiments with aqueous solution of 10:1 (v/v)% APTES/DMOAP mixtures to provide both homeotropic orientation and sufficient amount of APTES molecules for immobilization of aptamers.

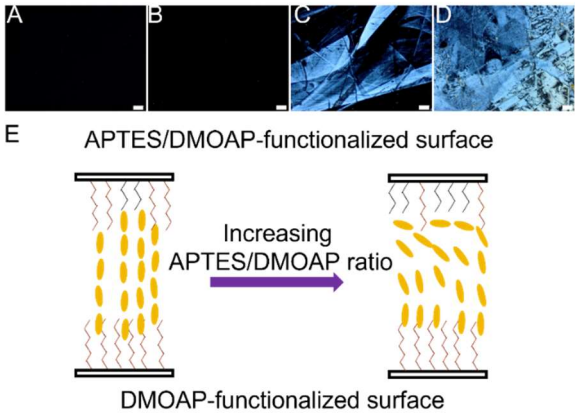

Figure 4.16 Polarized optical micrographs of LC sandwich cells where LC is sandwiched between a bottom surface functionalized with 1% DMOAP and upper surface functionalized with various (v/v)% APTES/DMOAP solutions, (A) (5:1) in water (B) (10:1) in water, (C) (20:1) in water, and (D) (5:1) in absolute ethanol,. Scale bars: 200 µm. (E) Representative schematic illustrations of LC configuration in the optical cell where upper surface functionalized with different ratios of APTES/DMOAP mixtures.

To facilitate aptamer immobilization, we used GA crosslinking method.[1,63,64] There should be enough GA molecules to immobilize aptamer on the APTES/DMOAP-functionalized glass surfaces. However, excess amounts leads to the crosslinking between APTES molecules which disrupts the homeotropic LC configuration and directly affects the response of the sensor.[1,5,6] Therefore, we conducted the experiments with 1 (v/v)% aqueous GA solutions considering the literature values

and obtained uniform homeotropic anchoring prior to aptamer immobilization (Figure 4.17).[1,5,6]

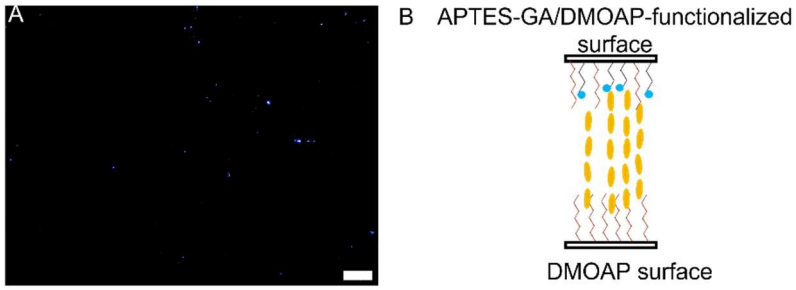

Figure 4.17 (A) Polarized optical micrograph of LC sandwich cell where LC is sandwiched between a bottom surface functionalized with 1% DMOAP and upper surface functionalized with 10:1 (v/v) % APTES/DMOAP aqueous solution and 1% (v/v) GA aqueous solution. Scale bar: 200 µm, and (B) Representative schematic illustration of LC configuration in the optical cell where upper glass surface functionalized with GA.

Lastly, we immobilized neomycin aptamer on glass surfaces via active aldehyde groups provided by GA which reacts to form amine linkage with the amine groups of the aptamer.[63] Similarly, homeotropic alignment of LC is disrupted as the concentration of aptamer was increased (Figure 4.18D).[1,5,6] Thus, aptamer concentration should also be optimized to have uniform homeotropic LC anchoring before target binding and sufficient enough to disturb the LC orientation after binding with its target molecule. For these purposes, we used RNA and DNA neomycin aptamers. Although we obtained mostly dark appearances under POM which is the indicative of homeotropic anchoring of LCs, we also observed bright appearance in some spots indicating the planar/tilted anchoring of LCs in our experiments when the concentration of RNA aptamer was 1 µM as shown in Figure 4.18Ai-ii. Considering the influence of surface density of aptamers on LC orientation, we decreased the RNA aptamer concentration to 100 nM and obtained uniform homeotropic anchoring consistently in all aptamer-bound spots (Figure 4.18B). However, as we proceeded with subsequent experiments, we observed that it was not sufficient for neomycin B detection as we hypothesized that there was insufficient amount of "aptamer-target" complexes to induce ordering transition of

LCs from homeotropic to degenerate planar/tilted on the surface. Considering that DNA aptamers are known to have higher stability than RNA aptamers, we performed the same experiments with 1 µM DNA neomycin aptamer solution and obtained uniformly dark background which indicates the uniform homeotropic anchoring on the surface (Figure 4.18C).[33,36] Therefore, we conducted the rest of the experiments with 1 µM DNA aptamer for detection of neomycin B in aqueous media.

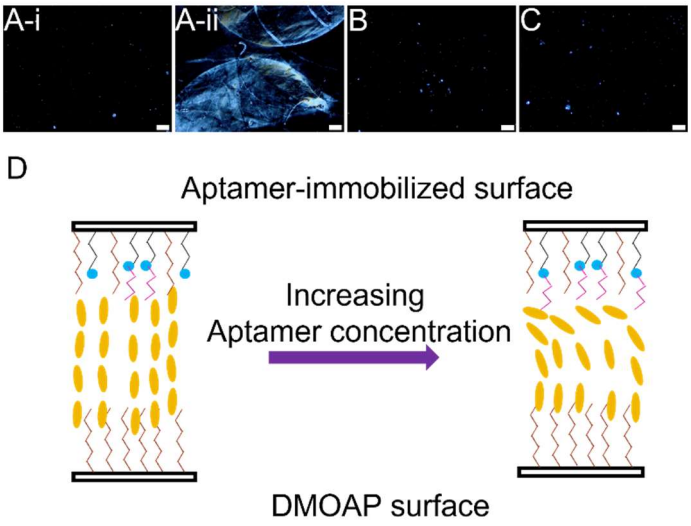

Figure 4.18 Polarized optical micrographs of LC sandwich cells after immobilization of aptamer on upper surface functionalized with 10:1 (v/v) % APTES/DMOAP aqueous solution and 1% (v/v) GA aqueous solution. (A(i-ii)) 1 µM RNA aptamer, (B) 100 nM RNA aptamer, (C) 1 µM DNA aptamer. Scale bar: 200 µm. (D) Representative schematic illustrations of LC configuration in the optical cell where upper surface immobilized with different concentrations of aptamer.

In summary, 10:1 (v/v) % APTES/DMOAP aqueous solution, 1% (v/v) GA aqueous solution and 1 µM DNA aptamer solution was determined as the optimal conditions to ensure that the change in optical response from dark to bright only results from the specific binding of neomycin aptamer to its target molecule.

4.2.1.2 Limit of Detection and Selectivity

After surface functionalizations and aptamer immobilization, we conducted experiments with a series of neomycin B concentrations to determine the detection

limit of developed LC-based aptasensing platform. With the perturbation of LC mesogens caused by the formation of aptamer-target complexes, we observed bright areas under POM resulting from the orientation transition from homeotropic to degenerate planar/tilted as described in Figure 4.15C, which reported the response of the sensor. We carried out experiments in between 0-50 µM neomycin B concentrations (Figure 4.19). When the concentration of neomycin B was 50, 5 or 0.5 µM, we observed bright appearances when we visualized optical cells under POM because of the conformational change of aptamers on the surface upon binding consistent with literature (Figure 4.19A-C).[1,5,6] Since the functionalized glass surface was exposed to the target solution as a circular drop covering three smaller aptamer-immobilized spots, the dark regions outside the circular bright spots proved that the orientation transition from homeotropic to degenerate planar/tilted was due to the aptamer binding to its target which was imaged as bright appearances under POM. With further decrease in neomycin B concentration, we observed fully dark backgrounds indicating that there were no sufficient aptamer-target complexes to disturb the LC orientation from homeotropic (Figure 4.19D-F). Based on these results, we determined the limit of detection as in between 50-500 nM neomycin B concentrations (Figure 4.19C-D). Qualitative analysis of polarized optical images indicated that decrease in the target concentration resulted in decrease in brightness of optical signal visualized under POM which was further investigated quantitatively by using ImageJ software (results below).

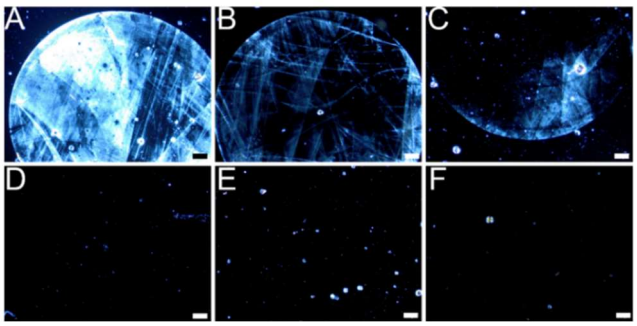

Figure 4.19 Polarized optical micrographs of LC sandwich cells after incubation with various neomycin B concentrations in PBS buffer: (A) 50 µM, (B) 5 µM, (C) 0.5 µM, (D) 0.05 µM, (E) 0.005 µM, and (F) 0 µM. Scale bars: 200 µm.

Next, we carried out experiments with competing target molecules for the comprehension of the specificity of the LC-based biosensor. We chose ampicillin as the interfering agent based on the selection of similar compound, antibiotics and proteins in past examples.[1,5,69,70] As shown in Figure 4.20A-D-panels *i*, interference color intensities of target mixtures were more significant compared to the intensities of surfaces incubated in target solutions with changing ampicillin concentrations (Figure 4.20A-D-panels *ii*). Additionally, as the ampicillin concentration in target mixture containing 5 μM of neomycin B was decreased, we qualitatively observed from the polarized optical images that brightness was also decreased. Also, we observed less bright areas in between the outer regions of aptamer-immobilized spots when we incubated functionalized glass surfaces with target mixture as evident representatively in Figure 4.20C-i. However, we did not observe these bright areas in between the outer regions of aptamer-immobilized spots when we exposed the sandwich cells to both neomycin B and ampicillin solutions separately (Figure 4.19 and Figure 4.20A-Dii). Also, we observed configuration transition of LC molecules from homeotropic to planar/tilted when we exposed the flat cells to decreasing concentrations of ampicillin (Figure 4.20A-Di). It is known that aptamer activity is dependent on their immobilization surfaces and procedures due to the strong effect on the conformation of aptamers.[71,72] Also, neomycin B is known to be freely soluble in water with higher solubility compared to ampicillin which is moderately soluble in water.[73–77] Therefore, we speculated that interaction between the aptamer-immobilized spots on glass surfaces with either target mixture of neomycin B and ampicillin or target solution containing only ampicillin might have resulted in the conformational changes of aptamers which resulted in higher brightness values. As another hypothesis, since we observed non-specific bindings in between the specific aptamer locations on glass slides (see Figure 4.20C-i), we hypothesized that ampicillin molecules were physically adsorbed on the functionalized glass surfaces due to its more hydrophobic nature compared to neomycin B and might not have been rinsed away which directly affects the LC configuration on these regions.[73–77] To check the validity of our hypothesis, we carried out quantitative analysis based

on the mean grayscale values of both the aptamer-immobilized spots and the outer regions between them.

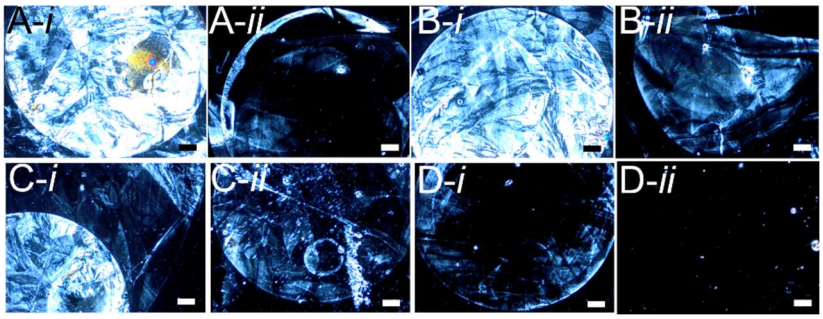

Figure 4.20 Polarized optical micrographs of LC sandwich cells after incubation with various target mixture concentrations in PBS buffer: (A) *i*- 5 µM neomycin B + 5 µM ampicillin, *ii*- 5 µM ampicillin, (B) *i*- 5 µM neomycin B + 0.5 µM ampicillin, *ii*- 0.5 µM ampicillin, (C) *i*- 5 µM neomycin B + 0.05 µM ampicillin, *ii*- 0.05 µM ampicillin, and (D) *i*- 5 µM neomycin B + 0.005 µM ampicillin, *ii*- 0.005 µM ampicillin. Scale bars: 200 µm.

For a quantitative analysis, we measured the mean grayscale values of POM results of different target solutions with varying concentrations by using ImageJ (Figure 4.21). It is evident from the measured quantities that, the grayscale intensity of bright areas gradually decreased as the target concentration decreased for all target solutions. Based on the qualitative and quantitative analysis results, we observed that presence of ampicillin increased the signal of optical response. However, we could still recognize neomycin B even though ampicillin was present in the target mixture since we could differentiate the results of the target solutions with and without ampicillin (Figure 4.19, Figure 4.20A-Di and Figure 4.21A). In addition, measurements for the outer regions between the aptamer-immobilized spots also revealed the increase in mean grayscale intensities with the presence of ampicillin. We observed significant differences in intensities in regions between aptamer-immobilized spots when the surfaces were exposed to target mixtures containing neomycin B and ampicillin or ampicillin only compared to intensities for neomycin B only (Figure 4.21B). These results supported our hypothesis of physisorption of ampicillin molecules since there were no aptamers immobilized on these regions to bound specifically or non-specifically to neomycin B or ampicillin, respectively.

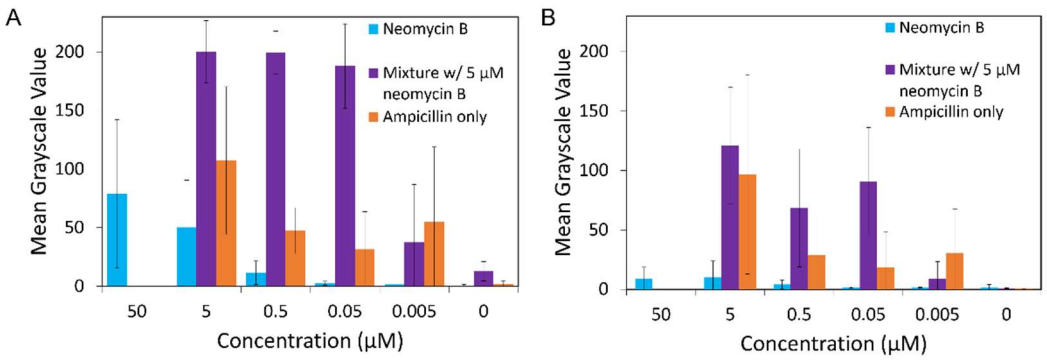

Figure 4.21 Mean grayscale values of LCs after incubation with various target solutions in PBS buffer, (A) Aptamer-immobilized spots, and (B) The outer regions between aptamer-immobilized spots. Target solutions: Neomycin B concentrations varying in between 50-0 µM (blue bars), mixture of 5 µM neomycin B + ampicillin concentrations varying in between 5-0.005 µM (purple bars) and, ampicillin concentrations varying in between 5-0.005 µM (orange bars).

4.2.2 Aptasensor in Microcapillaries

For aforementioned portability, easy quantification and affordable sensing purposes, we adapted the proposed procedure into glass microcapillaries. Schematic illustration of the method followed in this part of the study is given in Figure 4.22 below.

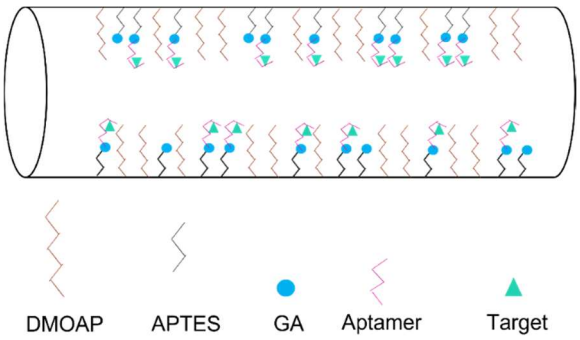

Figure 4.22 Schematic illustration of surface modified microcapillaries for aptasensing platform.

4.2.2.1 Surface Functionalization and Aptamer Immobilization on Inner Walls of Microcapillaries

We characterized the LC configuration on aptamer-immobilized flat surfaces before and after incubating the surfaces with various concentrations of target solutions in Chapter 4.2.1. However, we did not have a reference surface within microcapillaries since the entire inner surface was exposed to the same solution during incubations. Because of this aspect, we also carried out the characterizations of LC configuration for the surface treatment and functionalization conditions of microcapillary geometry. Characterizations of LC configurations within DMOAP-functionalized microcapillaries were performed for aqueous-LC interfaces in Chapter 4.1. In this section, we carried out the characterizations for the aptamer-immobilized microcapillary surfaces. Since the large aptamer-target complexes would result in the planar/tilted orientations of LC, we wanted to promote homeotropic anchoring of LC until the end of the aptamer immobilization step prior to target incubation as explained in Chapter 4.2.1. Also, as we investigated in Chapter 4.1, four-petal appearance was observed when the inner walls of microcapillary promote homeotropic anchoring of LC mesogens. Thus, we sought to keep the percentages of four-petal apperance of LC compartments confined in microcapillaries high until we exposed the inner surfaces to target solutions (Figure 4.23D). Based on the satisfactory results of surface functionalizations of flat glass slides, we preserved the 10:1 (v/v) % APTES/DMOAP aqueous solution and 1% (v/v) GA aqueous solution for the functionalization of inner walls of glass microcapillaries to give LC homeotropic anchoring at the inner walls since we observed four-petal appearances in every LC compartments confined in functionalized microcapillaries (Figure 4.23A, B). Although immobilization of 1 μM DNA aptamer solution provided sufficient binding sites without disturbing LC orientation in certain number of experiments, we observed inconsistency in our results. That is, when we treated the microcapillaries with piranha solution for 2 h, we observed the percentages of LC compartments showing four petal appearances as 70.4% and 50.5% for 500 nM and

1 μM DNA aptamer concentrations, respectively. It was essential to increase these low four-petal appearance percentages to ensure that the orientation transition to be the result of aptamer-target bindings which was expected to be the response of the sensor. Therefore, we extended the piranha solution cleaning period which was the first intervention to eliminate the surface contamination which might cause the discrepancy in results (Figure 4.23C, see also Figure 4.24D).

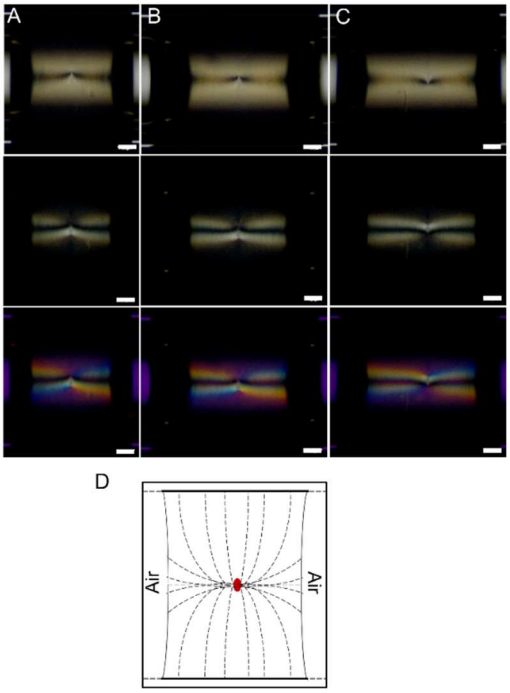

Figure 4.23 Bright field, polarized light and full-wave retardation plate optical micrographs of LCs confined in microcapillaries after incubation with (A) (10:1) APTES/DMOAP aqueous solution, (B) 1% (v/v) GA aqueous solution, and (C) immobilization of 1 μM DNA aptamer. Scale bars: 100 μm. (D) Schematic illustrations of LC configuration confined in microcapillaries whose inner walls were functionalized with APTES/DMOAP or GA or with aptamer immobilized on the surface.

Increasing the time for piranha treatment of glass microcapillaries enhanced the surface activity for immobilization of aptamers as evident from the percentages of four-petal appearance of LC compartments within capillaries. Four-petal appearance percentages increased 50.5% to 65.0% for 1 μM DNA aptamer concentration. Yet, further modifications were needed to increase the sensor performance. We

hypothesized that there can be two reasons for having four-petal appearance of 65.0% of LC compartments when we used 1 µM DNA aptamer solution for immobilization process; either there was no sufficient amount of aptamer to be immobilized on the glass surface or there was excess amount of aptamer which disrupted the LC configuration. To clarify, we conducted experiments with 2 µM and 500 nM DNA aptamer solutions. We observed that as the aptamer solution concentration decreased, percentage of homeotropic four-petal LC compartments gradually increased which were indicated as 47.6%, 65.0% and 88.7% for 2 µM, 1 µM and 500 nM DNA aptamer concentrations, respectively in Figure 4.24D. We obtained 88.7% homeotropic LC compartments when the aptamer solution concentration was 500 nM which can be further optimized (Figure 4.24A-C). Based on the four-petal appearance percentages with respect to DNA aptamer concentrations, we concluded that 1 µM DNA aptamer concentration was in excess amounts to be immobilized on the functionalized glass surfaces which resulted in configuration transition from homeotropic to degenerate planar/tilted. Thus, we continued the rest of the experiments with 500 nM DNA aptamer solutions.

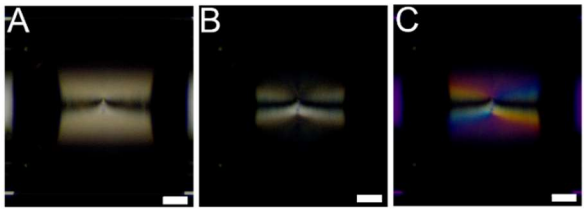

D

DNA Aptamer	2 µM	1 µM	500 nM
% Four-petal	47.6	65.0	88.7

Figure 4.24 (A) Bright field, (B) Polarized light, (C) Full-wave retardance optical micrographs of LCs confined in microcapillaries after immobilization of aptamer inner walls functionalized with 10:1 (v/v)% APTES/DMOAP aqueous solution, 1% (v/v) GA aqueous solution and 500 nM DNA aptamer. Scale bars: 100 µm. (D) Percentages of four-petal LC compartments within microcapillaries for 2 µM, 1 µM and 500 nM DNA aptamer concentrations.

4.2.2.2 Limit of Detection and Selectivity

After optimization of surface modifications for adaptation of aptasensing platform into microcapillaries, we incubated surface-treated microcapillaries into various neomycin B target concentrations to determine the detection limit of the sensor. With the formation of aptamer-target complexes, LC assumed planar anchoring near the inner walls of microcapillaries leading to configuration change from four-petal appearance consistent with the experiments carried out with planar cells which were discussed in Chapter 4.2.1. (Figure 4.25). When the concentration of neomycin B was 50, 5 or 0.5 μM, we observed degenerate planar/tilted anchoring of LC near the walls when we visualized under POM (Figure 4.25A-C). As neomycin B concentration was sequentially decreased, we observed four-petal appearances indicating that there were no sufficient aptamer-target complexes for perturbation of the LC orientation within LC compartments (Figure 4.25D-F). As can be seen from the quantitative analysis of the responses given in Figure 4.25G, percentages of planar LC compartments decreased with the decrease in the concentration of neomycin B. According to these results, we determined the limit of detection as in between 50-500 nM neomycin B concentrations for microcapillary-based aptasensor which was a similar concentration interval we determined for flat surface geometries.

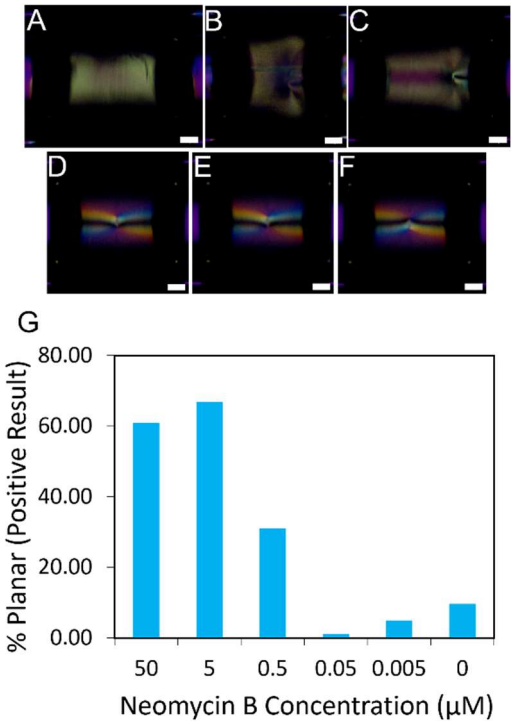

Figure 4.25 Polarized optical micrographs of LCs confined in microcapillaries after incubation with various neomycin B concentrations in PBS buffer: (A) 50 μM, (B) 5 μM, (C) 0.5 μM, (D) 0.05 μM, (E) 0.005 μM, and (F) 0 μM. Scale bar: 100 μm. (G) Percentages of planar LC compartments (denoted as positive result) within microcapillaries after incubation with various neomycin B concentrations in PBS buffer.

For the determination of specificity, we conducted experiments with target mixtures of 5 μM neomycin B and various concentrations of ampicillin varying in between 5-0.005 μM as we performed in flat sandwich cells. Similar with sandwich cell-based aptasensor, we qualitatively observed increase in configuration transition from four-petal appearance with the interference of ampicillin (Figure 4.26). In all experiments we conducted with the mixture of 5 μM neomycin B and 5 μM ampicillin, we observed degenerate planar/tilted LC compartments within the whole microcapillaries (concluded from the disappearance of the four-petal appearance) although the percentages of degenerate planar/tilted LC compartments were 66.7% when the microcapillaries were exposed to 5 μM neomycin B only (Figure 4.25G). As we also discussed for the flat sandwich cells in Chapter 4.2.1, we observed a gradual decrease in the percentages of planar LC compartments when we incubated

the microcapillaries in the target mixtures containing 5 µM neomycin B and decreasing concentrations of ampicillin. Also, in some of the experiments, we observed degenerate planar/tilted LC compartments when we exposed the microcapillaries to 5 µM ampicillin only. Similar to the results of flat cells, these results led us to hypothesize that due to changes on the surface caused by the interaction of neomycin B and ampicillin or the physisorption of ampicillin on the glass surfaces, the sensor response was affected.

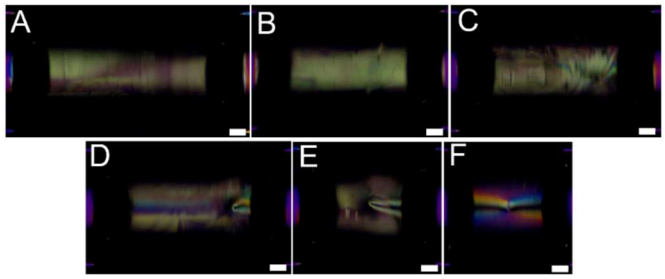

Figure 4.26 Polarized optical micrographs of LCs confined in microcapillaries after incubation with various target solution concentrations in PBS buffer: (A) 5 µM neomycin B + 5 µM ampicillin, (B) 5 µM neomycin B + 0.5 µM ampicillin, (C) 5 µM neomycin B + 0.05 µM ampicillin, (D) 5 µM neomycin B + 0.005 µM ampicillin, and (E) 5 µM ampicillin. (F) Representative negative response of the microcapillary-based sensor, capillaries were incubated in 5 µM ampicillin solution. Scale bars: 100 µm.

For the target incubation results, we denoted the planar LC configuration as positive response. The quantitative analysis of configuration of LC compartments revealed that presence of ampicillin was altered the sensor response with gradual decrease in planar compartments with respect to decreasing ampicillin concentrations (Figure 4.27, purple bars). In accordance with the sandwich cell-based aptasensor results, positive response percentages of LC compartments were increased when the microcapillaries were incubated in various target mixtures consisting of 5 µM neomycin B and 5 µM and 0.5 µM concentrations of ampicillin compared to target solution containing 5 µM neomycin B only (Figure 4.27, purple bars, see also Figure 4.25G). We also observed planar LC compartments when we exposed the microcapillaries to 5 µM ampicillin only (Figure 4.27, orange bar). These results strengthened our pre-mentioned hypotheses which we stated in Chapter 4.2.1 that

the mixtures of neomycin B and ampicillin disturbed the response of the sensor which could be due to the conformational change of aptamer or physisorption phenomenon due to more hydrophobic nature of ampicillin compared to neomycin B.[73–77]

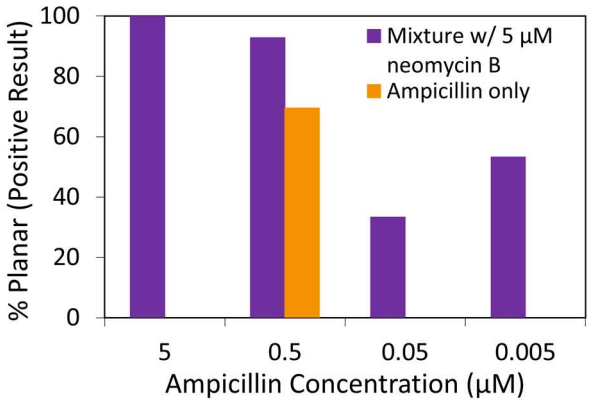

Figure 4.27 Percentages of planar LC compartments (denoted as positive result) within microcapillaries after incubation with various target solutions in PBS buffer. Target solutions: Mixture of 5 µM neomycin B + ampicillin concentrations varying in between 5-0.005 µM (purple bars) and, 5 µM ampicillin concentration (orange bar).

CHAPTER 5

CONCLUSION

In the first part of this thesis study, we demonstrated a new method for LC microcapillary-based sensor. Unlike other LC-based methods used for sensing applications, our method provides opportunity to control the species at both LC-aqueous interfaces of the LC compartment confined in microcapillary, which can be used for the quantification of ordering transition resulting from the interactions at LC-water interfaces. The method proposed in this thesis study offers reversible and continuous use and allows to observe the time-dependent ordering transition within the LC phase that would also provide fundamental information beyond the application-wise needs.

The LC compartment-based system we introduce in the first part is new and it can be further developed for selective response against analytes from complex mixtures. Either the LC-solid interface or LC-aqueous interface can be used for such purposes using the methods developed so far.[11] In the second part of this thesis study, we demostrated a label-free liquid crystal-based aptasensor to be used in both flat and microcapillary geometries for the detection of neomycin B. We successfully functionalized the glass surfaces with 10:1 (v/v)% APTES/DMOAP aqueous solution, 1 (v/v)% GA aqueous solution to create reactive sites for aptamer immobilization. We used 1 μM and 500 nM DNA aptamer solutions for flat and microcapillaries, respectively. We exposed the developed aptasensors to various concentrations of target solutions containing either neomycin B or ampicillin or the mixture containing both neomycin B and ampicillin. With the formation of aptamer-target complexes, we observed orientation transition from homeotropic to planar which we visualized under crossed polarizers. We characterized the LC response according to the polarized optical images. Qualitative and quantitative analyses were

done for both geometries. The detection limit for both flat cells and microcapillaries were determined to be in between 50-500 nM neomycin B concentrations. According to the qualitative and quantitative results of both geometries, we hypothesized that interaction between neomycin B and ampicillin molecules directly affected the LC configuration which might be due to conformational change of the aptamers which were immobilized on the glass surfaces or physisorption of ampicillin due to more hydrophobicity compared to neomycin B.

Beyond the findings and the implications that were reported here, we propose future directions that might be of a broad interest. For the first part of our thesis study, first, the compartment sizes and the positioning that we used were random. However, a control over such is required for future developments. Current literature may offer additional opportunities for such purposes using lithography techniques.[78] Second, we concluded that the motion of the defects within the LC compartments were driven via elastic interactions. Well-defined LC compartments and a control over the surface anchoring independently at the two ends of the LC compartments would also provide opportunities for careful investigation of the elastic forces acting on the defects and their influence on the motion and the structural transitions. Lastly, the system we developed herein can be integrated into flow systems to track the temporal and cumulative profiles. For the second part, the effect of the presence of ampicillin as the interfering agent on the specific binding of neomycin aptamer to its target can be investigated further with respect to decreasing ampicillin concentrations in the target solutions containing various concentrations of neomycin B. In addition, to understand the interaction between the surface and target molecules, various target molecules with different characteristics can be used for the specificity measurements of proposed aptasensing platforms.

The methods and the systems that we develop herein are promising considering their simplicity, the ease of quantification, and their portability. To sum, we introduced microcapillary-based systems with negligible cost that may facilitate widespread use after further developments. The findings published in this thesis can further be used to develop sensors for specific purposes that require continuous tracking of the

chemical and biological species that is critical for the health and safety of the individuals and society.

REFERENCES

1. Ren, H., An, Z. & Jang, C. H. Liquid crystal-based aptamer sensor for sensitive detection of bisphenol A. *Microchem. J.* **146**, 1064–1071 (2019).

2. Mehlhorn, A., Rahimi, P. & Joseph, Y. Aptamer-based biosensors for antibiotic detection: A review. *Biosensors* **8**, (2018).

3. Munir, S., Khan, M. & Park, S. Y. Bienzyme liquid-crystal-based cholesterol biosensor. *Sensors Actuators, B Chem.* **220**, 508–515 (2015).

4. Carlton, R. J. *et al.* Chemical and biological sensing using liquid crystals. *Liq. Cryst. Rev.* **1**, 29–51 (2013).

5. Rouhbakhsh, Z., Verdian, A. & Rajabzadeh, G. Design of a liquid crystal-based aptasensing platform for ultrasensitive detection of tetracycline. *Talanta* **206**, 120246 (2020).

6. Wang, Y., Wang, B., Shen, J., Xiong, X. L. & Deng, S. X. Aptamer based bare eye detection of kanamycin by using a liquid crystal film on a glass support. *Microchim. Acta* **184**, 3765–3771 (2017).

7. Nguyen, D. K. & Jang, C. H. An acetylcholinesterase-based biosensor for the detection of pesticides using liquid crystals confined in microcapillaries. *Colloids Surfaces B Biointerfaces* **200**, 111587 (2021).

8. Nguyen, D. K. & Jang, C. H. A Cationic Surfactant-Decorated Liquid Crystal-Based Aptasensor for Label-Free Detection of Malathion Pesticides in Environmental Samples. *Biosensors* **11**, 1–4 (2021).

9. An, Z. & Jang, C. H. Sensitive and selective method for detecting cysteine based on optical properties of liquid crystal. *Sensors Actuators, B Chem.* **269**, 135–142 (2018).

10. Lagerwall, J. P. F. An Introduction to the Physics of Liquid Crystals. in *Fluids,*

Colloids and Soft Materials: An Introduction to Soft Matter Physics 307–340 (2016). doi:10.1002/9781119220510.ch16.

11. Bukusoglu, E., Bedolla Pantoja, M., Mushenheim, P. C., Wang, X. & Abbott, N. L. Design of Responsive and Active (Soft) Materials Using Liquid Crystals. *Annu. Rev. Chem. Biomol. Eng.* **7**, 163–196 (2016).

12. Zhong, S. & Jang, C. H. Highly sensitive and selective glucose sensor based on ultraviolet-treated nematic liquid crystals. *Biosens. Bioelectron.* **59**, 293–299 (2014).

13. Khan, M. & Park, S. Y. Liquid crystal-based proton sensitive glucose biosensor. *Anal. Chem.* **86**, 1493–1501 (2014).

14. Khan, M. & Park, S. Y. Liquid crystal-based glucose biosensor functionalized with mixed PAA and QP4VP brushes. *Biosens. Bioelectron.* **68**, 404–412 (2015).

15. Chen, C. H., Lin, Y. C., Chang, H. H. & Lee, A. S. Y. Ligand-doped liquid crystal sensor system for detecting mercuric ion in aqueous solutions. *Anal. Chem.* **87**, 4546–4551 (2015).

16. Hu, Q. Z. & Jang, C. H. Liquid crystal-based sensors for the detection of heavy metals using surface-immobilized urease. *Colloids Surfaces B Biointerfaces* **88**, 622–626 (2011).

17. Brake, J. M. & Abbott, N. L. An experimental system for imaging the reversible adsorption of amphiphiles at aqueous-liquid crystal interfaces. *Langmuir* **18**, 6101–6109 (2002).

18. Brake, J. M., Mezera, A. D. & Abbott, N. L. Active control of the anchoring of 4’-pentyl-4-cyanobiphenyl (5CB) at an aqueous-liquid crystal interface by using a redox-active ferrocenyl surfactant. *Langmuir* **19**, 8629–8637 (2003).

19. Brake, J. M., Mezera, A. D. & Abbott, N. L. Effect of surfactant structure on the orientation of liquid crystals at aqueous-liquid crystal interfaces.

Langmuir **19**, 6436–6442 (2003).

20. Lockwood, N. A., De Pablo, J. J. & Abbott, N. L. Influence of surfactant tail branching and organization on the orientation of liquid crystals at aqueous-liquid crystal interfaces. *Langmuir* **21**, 6805–6814 (2005).

21. Hartono, D., Xue, C. Y., Yang, K. L. & Yung, L. Y. L. Decorating liquid crystal surfaces with proteins for real-time detection of specific protein-protein binding. *Adv. Funct. Mater.* **19**, 3574–3579 (2009).

22. Khan, W. & Park, S. Y. Configuration change of liquid crystal microdroplets coated with a novel polyacrylic acid block liquid crystalline polymer by protein adsorption. *Lab Chip* **12**, 4553–4559 (2012).

23. Park, J. S. & Abbott, N. L. Ordering transitions in thermotropic liquid crystals induced by the interfacial assembly and enzymatic processing of oligopeptide amphiphiles. *Adv. Mater.* **20**, 1185–1190 (2008).

24. Brake, J. M., Daschner, M. K., Luk, Y. & Abbott, N. L. Biomolecular Interactions at Phospholipid-Decorated Surfaces of Liquid Crystals. *Science.* **302**, 2094–2098 (2003).

25. Lin, I. *et al.* Endotoxin-Induced Structural Transformations in Liquid Crystalline Droplets. *Science.* **332**, 1297–1300 (2011).

26. Han, G. R., Song, Y. J. & Jang, C. H. Label-free detection of viruses on a polymeric surface using liquid crystals. *Colloids Surfaces B Biointerfaces* **116**, 147–152 (2014).

27. Sivakumar, S., Wark, K. L., Gupta, J. K., Abbott, N. L. & Caruso, F. Liquid crystal emulsions as the basis of biological sensors for the optical detection of bacteria and viruses. *Adv. Funct. Mater.* **19**, 2260–2265 (2009).

28. Manna, U. *et al.* Liquid Crystal Chemical Sensors That Cells Can Wear. *Angew. Chemie* **125**, 14261–14265 (2013).

29. Lin, I. H. *et al.* Endotoxin-induced structural transformations in liquid crystalline droplets. *Science.* **332**, 1297–1300 (2011).

30. Smith, A. D., Abbott, N. & Zavala, V. M. Convolutional Network Analysis of Optical Micrographs for Liquid Crystal Sensors. *J. Phys. Chem. C* **124**, 15152–15161 (2020).

31. Cao, Y., Yu, H., Abbott, N. L. & Zavala, V. M. Machine Learning Algorithms for Liquid Crystal-Based Sensors. *ACS Sensors* **3**, 2237–2245 (2018).

32. Şengül, S., Aydoğan, N. & Bukusoglu, E. Nanoparticle Adsorption Induced Configurations of Nematic Liquid Crystal Droplets. *J. Colloid Interface Sci.* (2021) doi:10.1016/j.jcis.2021.10.156.

33. Ilgu, M., Fazlioglu, R., Ozturk, M., Ozsurekci, Y. & Nilsen-Hamilton, M. Aptamers for Diagnostics with Applications for Infectious Diseases. *Recent Adv. Anal. Chem.* (2019) doi:10.5772/intechopen.84867.

34. Keefe, A. D., Pai, S. & Ellington, A. Aptamers as therapeutics. *Nat. Rev. Drug Discov.* **9**, 537–550 (2010).

35. Marrazza, G. Aptamer Sensors. *Biosensors* **7**, 5–7 (2017).

36. Ozturk, M., Nilsen-hamilton, M. & Ilgu, M. Aptamer Applications in Neuroscience. (2021).

37. Popov, N., Smirnova, A., Usol'tseva, N. & Popov, P. Determination of concentrations of surface-active materials in aqueous solutions at different pH values using liquid crystals. *Zhidkie Krist. i Ikh Prakt. Ispol'zovanie* **17**, 34–42 (2017).

38. Tan, H., Yang, S., Shen, G., Yu, R. & Wu, Z. Signal-enhanced liquid-crystal DNA biosensors based on enzymatic metal deposition. *Angew. Chemie - Int. Ed.* **49**, 8608–8611 (2010).

39. Lai, S. L. & Yang, K. L. Detecting DNA targets through the formation of

DNA/CTAB complex and its interactions with liquid crystals. *Analyst* **136**, 3329–3334 (2011).

40. Avşar, D. I. & Bukusoglu, E. Chameleon skin-inspired polymeric particles for the detection of toluene vapor. *Soft Matter* 8683–8691 (2020) doi:10.1039/d0sm01289k.

41. Clare, B. H. & Abbott, N. L. Orientations of nematic liquid crystals on surfaces presenting controlled densities of peptides: Amplification of protein-peptide binding events. *Langmuir* **21**, 6451–6461 (2005).

42. Chen, C. H. & Yang, K. L. Detection and quantification of DNA adsorbed on solid surfaces by using liquid crystals. *Langmuir* **26**, 1427–1430 (2010).

43. Bai, Y. & Abbott, N. L. Enantiomeric interactions between liquid crystals and organized monolayers of tyrosine-containing dipeptides. *J. Am. Chem. Soc.* **134**, 548–558 (2012).

44. Brake, Jeffrey M.; Daschner, Maren; K. Luk, Y. & Abbott, N. L. Biomolecular Interactions at Phospholipid-Decorated Surfaces of Liquid Crystals. **302**, 2094–2098 (2003).

45. Shah, R. R. & Abbott, N. L. Principles for measurement of chemical exposure based on recognition-driven anchoring transitions in liquid crystals. *Science.* **293**, 1296–1299 (2001).

46. Price, A. D. & Schwartz, D. K. DNA hybridization-induced reorientation of liquid crystal anchoring at the nematic liquid crystal/aqueous interface. *J. Am. Chem. Soc.* **130**, 8188–8194 (2008).

47. Yang, Z. & Abbott, N. L. Spontaneous formation of water droplets at oil-solid interfaces. *Langmuir* **26**, 13797–13804 (2010).

48. Gupta, J. K., Zimmerman, J. S., De Pablo, J. J., Caruso, F. & Abbott, N. L. Characterization of adsorbate-induced ordering transitions of liquid crystals within monodisperse droplets. *Langmuir* **25**, 9016–9024 (2009).

49. Miller, D. S., Wang, X., Buchen, J., Lavrentovich, O. D. & Abbott, N. L. Analysis of the internal configurations of droplets of liquid crystal using flow cytometry. *Anal. Chem.* **85**, 10296–10303 (2013).

50. Wei, Y. & Jang, C. H. Selective and direct detection of free amino acid using the optical birefringent patterns of confined nematic liquid crystals. *Liq. Cryst.* **44**, 303–311 (2017).

51. Zhong, S. & Jang, C. H. Nematic liquid crystals confined in microcapillaries for imaging phenomena at liquid-liquid interfaces. *Soft Matter* **11**, 6999–7004 (2015).

52. Jiang, S. *et al.* Using machine learning and liquid crystal droplets to identify and quantify endotoxins from different bacterial species. *Analyst* **146**, 1224–1233 (2021).

53. Sachan, A., Ilgu, M., Kempema, A., Kraus, G. A. & Nilsen-Hamilton, M. Specificity and Ligand Affinities of the Cocaine Aptamer: Impact of Structural Features and Physiological NaCl. *Anal. Chem.* **88**, 7715–7723 (2016).

54. Lockwood, N. A., Gupta, J. K. & Abbott, N. L. Self-assembly of amphiphiles, polymers and proteins at interfaces between thermotropic liquid crystals and aqueous phases. *Surf. Sci. Rep.* **63**, 255–293 (2008).

55. Škarabot, M., Osmanagič, E. & Muševič, I. Surface anchoring of nematic liquid crystal 8OCB on a DMOAP-silanated glass surface. *Liq. Cryst.* **33**, 581–585 (2006).

56. Kahn, F. J., Taylor, G. N. & Schonhorn, H. Surface-Produced Alignment of Liquid Crystals. *Proc. IEEE* **61**, 823–828 (1973).

57. Allender, D. W., Crawford, G. P. & Doane, J. W. Determination of the liquid-crystal surface elastic constant K24. *Phys. Rev. Lett.* **67**, 1442–1445 (1991).

58. Burylov, S. V. Equilibrium configuration of a nematic liquid crystal confined

to a cylindrical cavity. *J. Exp. Theor. Phys.* **85**, 873–886 (1997).

59. Kralj, S. & Žumer, S. Saddle-splay elasticity of nematic structures confined to a cylindrical capillary. *Phys. Rev. E* **51**, 366–370 (1995).

60. Wang, X. *et al.* Experimental Insights into the Nanostructure of the Cores of Topological Defects in Liquid Crystals. *Phys. Rev. Lett.* **116**, 1–5 (2016).

61. Sonnet, A. M. & Virga, E. G. Flow and reorientation in the dynamics of nematic defects. *Liq. Cryst.* **36**, 1185–1192 (2009).

62. Honaker, L. W., Lagerwall, J. P. F. & Jampani, V. S. R. Microfluidic Tensiometry Technique for the Characterization of the Interfacial Tension between Immiscible Liquids. *Langmuir* **34**, 2403–2409 (2018).

63. Gunda, N. S. K., Singh, M., Norman, L., Kaur, K. & Mitra, S. K. Optimization and characterization of biomolecule immobilization on silicon substrates using (3-aminopropyl)triethoxysilane (APTES) and glutaraldehyde linker. *Appl. Surf. Sci.* **305**, 522–530 (2014).

64. Marques, M. E., Mansur, A. A. P. & Mansur, H. S. Chemical functionalization of surfaces for building three-dimensional engineered biosensors. *Appl. Surf. Sci.* **275**, 347–360 (2013).

65. Kulkarni, S. A., Ogale, S. B. & Vijayamohanan, K. P. Tuning the hydrophobic properties of silica particles by surface silanization using mixed self-assembled monolayers. *J. Colloid Interface Sci.* **318**, 372–379 (2008).

66. Tong, Y. *et al.* Preferential adsorption of amino-terminated silane in a binary mixed self-assembled monolayer. *Langmuir* **27**, 5420–5426 (2011).

67. Stranick, S. J., Parikh, A. N., Tao, Y. T., Allara, D. L. & Weiss, P. S. Phase separation of mixed-composition self-assembled monolayers into nanometer scale molecular domains. *J. Phys. Chem.* **98**, 7636–7646 (1994).

68. Pasternack, R. M., Amy, S. R. & Chabal, Y. J. Attachment of 3-

(aminopropyl)triethoxysilane on silicon oxide surfaces: Dependence on solution temperature. *Langmuir* **24**, 12963–12971 (2008).

69. Bala, R., Kumar, M., Bansal, K., Sharma, R. K. & Wangoo, N. Ultrasensitive aptamer biosensor for malathion detection based on cationic polymer and gold nanoparticles. *Biosens. Bioelectron.* **85**, 445–449 (2016).

70. Li, X. *et al.* Aptamer-based liquid crystal biosensor for detection of platelet-derived growth factor BB. *Fenxi Huaxue/ Chinese J. Anal. Chem.* **42**, 629–635 (2014).

71. Tello, A., Cao, R., Marchant, M. J. & Gomez, H. Conformational Changes of Enzymes and Aptamers Immobilized on Electrodes. *Bioconjug. Chem.* **27**, 2581–2591 (2016).

72. Macdonald, H. *et al.* Influence of Aptamer Surface Coverage on Small Target Recognition: A SPR and QCM-D Comparative Study. *J. Phys. Chem. C* **123**, 13561–13568 (2019).

73. Florey, K., Atwater, N. W., Brewer, G. A., Chafetz, L. & Fusari, S. A. *Analytical Profiles of Drug Substances*. *Microchemical Journal* vol. 2 (1973).

74. Florey, K. *et al. Analytical Profiles of Drug Substances*. vol. 8 (1979).

75. Lodhi, Shahid, Weiner, Norman D., Schacht, J. Interactions of Neomycin with Monomolecular Films of Polyphosphoinositides and Other Lipids. *Biochim. Biophys. Acta - Biomembr.* **557**, (1979).

76. Yamaguchi, A., Hiruma, R. & Sawai, T. The effect of hydrophobicity of β-lactam antibiotics on their phospholipid bilayer permeability. *FEBS Lett.* **164**, 389–392 (1983).

77. Keswani, N., Choudhary, S. & Kishore, N. Interaction of weakly bound antibiotics neomycin and lincomycin with bovine and human serum albumin: Biophysical approach. *J. Biochem.* **148**, 71–84 (2010).

78. Zhang, Y., Van Nieuwkasteele, J. W., Qiang, M., Tsai, P. A. & Lammertink, R. G. H. Spatial Site-Patterning of Wettability in a Microcapillary Tube. *ACS Appl. Mater. Interfaces* **8**, 10657–10660 (2016).